SEDIMENTARY EVOLUTION AND DISTRIBUTION OF BENTHIC FAUNA OF AN APTIAN PROTECTED BAY (OLIETE SUBBASIN, SPAIN)

A. García-Penas [a, *], M. Aurell [a] and S. Zamora [a,b]

[a] Grupo Aragosaurus-IUCA, 1Departamento de Ciencias de la Tierra, Facultad de Ciencias, Universidad de Zaragoza, C/Pedro Cerbuna, 12, 50009, Zaragoza, Spain

[b] Instituto Geológico y Minero de España (IGME-CSIC), Residencia CSIC, Campus Aula Dei, Av. Montañana 1005, E-50059, Zaragoza, Spain, (orcid.org/0000-0002-3917-4628)

*Corresponding author

E-mail addresses: alvarogpenas@gmail.com (A. García-Penas), maurell@unizar.es (M. Aurell), s.zamora@igme.es (S. Zamora)

Keywords

Early Cretaceous, palaeoenvironment, palaeogeography, sequence stratigraphy, faunal assemblages

Abstract

Detailed facies and sequence stratigraphic analysis of an Aptian shallow-marine succession illustrates the evolution of sedimentary environments and their benthic faunal associations in a marginal bay developed in northeastern Iberia (Maestrazgo Basin, Oliete Subbasin). In this bay, marine circulation was hampered by wide stationary shoals located in the low-subsidence transitional areas between subbasins. The Aptian sedimentary record of this bay (Josa and Oliete formations) is composed of four transgressive-regressive (T-R) sequences bounded by major unconformities generated during relative sea-level falls. The Josa Fm (formally defined herein) encompasses an asymmetrical T-R cycle (sequence J). It comprises transgressive prodelta clays with episodic orbitolinid blooms, grading upwards to regressive freshwater-influenced littoral and delta-front sandstones and sandy limestones which yield diverse bivalve communities dominated by trigoniids. The Oliete Fm encompasses three T-R cycles (sequences O1-O3), mostly

deposited in a protected lagoon. The transgressive hemicycle of each sequence is dominated by marls containing low-diversity faunal associations composed of ostracods and mm-sized gastropods and bivalves, indicating stressed (probably dysoxic) conditions in the deepest parts of the lagoon, related to a lack of water circulation. The regressive hemicycle of sequences O1 and O2 is characterised by low-energy intertidal to shallow subtidal deposits including sponge spiculites, mud-dominated accumulations of articulated bivalves and gastropods with low-diversity microfaunal associations composed mainly of *Choffatella* and few other textulariids, and marginal oyster-serpulid patches. The uppermost part of Sequence O2 is characterised by the development of siliciclastic tide-influenced coastal plains. Sequence O3 consists of massive intertidal to shallow subtidal glauconite accumulations related to the transgressive reworking of siliciclastic deposits. Foraminiferal associations in Sequence O3 show an increase in diversity (including miliolids, lageniids and diverse textulariids), which was probably fostered by a more stable connection with open seas, caused by tectonic activity in the bounding shoal areas. The analysis of these four sequences represents a comprehensive and detailed characterization of shallow-to-marginal marine benthic communities integrated in a sequence stratigraphic framework.

1 Introduction

The transgressive flooding of low-relief coastal areas can give rise to a wide variety of coastal shallow-marine features, such as bays, estuaries and lagoons (Kjerfve, 1994; Duck and da Silva, 2012). The persistence in time of these coastal features depends directly on the local relative rate of sea-level change, which frequently makes them short-lived on a geologic time frame and prone to rapid environmental variations (Kjerfve, 1994). Furthermore, quickly changing sedimentary dynamics often result in patchy, non-linear spatial distribution patterns of sediments, referred to as facies mosaics (Wright and Burgess, 2005).

Semi-enclosed bays are marginal marine environments defined by their limited communication with open seas, which renders them prone to environmental stress derived from reduced water circulation and variations in freshwater input (e.g. Hobday et al., 1979; Gravina et al., 1989; Kelble et al., 2007; Xia and Jiang, 2015). Acting as interface between land and sea, these marginal marine settings also offer a unique insight into the interplay among sediment supply, sea level and climate, and the biotic response to the variations of these factors. This study focuses on the Barremian-Aptian marine sedimentary record of the Oliete Subbasin (NE Spain), which records the evolution of a semi-enclosed bay with a varying degree of connection to shallow open seas. In a context of global climatic instability (Dumitrescu, 2006; Hay and Floegel, 2012; Huck and Heimhofer, 2021; Hasegawa et al., 2022) characterised by large-scale eustatically-driven sea-level oscillations (Bover-Arnal et al., 2016, 2022; Haq, 2014; Immenhauser, 2005), the Barremian-Aptian Oliete Subbasin developed a variety of sedimentary environments, from open-marine to protected carbonate lagoons and siliciclastic coastal plains. These environments were inhabited by specific benthic faunal communities, which are markedly different from their coeval counterparts in adjacent shallow-marine areas. In the wide spectrum of available sedimentological and palaeontological methods, analysis of macro and microfaunal associations stands out for its applicability as a tool to understand the interplay of environmental factors in marginal environments (e.g. Fürsich and Kirkland, 1986; Fürsich et al., 1995; Yin et al., 1995). Thus, the Oliete Subbasin offers a unique opportunity to study the response of benthic faunal associations to changes in a wide array of environmental factors in proximal settings, as well as to characterise the variations of such associations in time and space following an up-to-date sequence-stratigraphic framework.

The specific aims of this work are (1) to carry out a detailed facies analysis of the Aptian stratigraphic record of the Oliete Subbasin, focusing on the vertical stacking patterns and lateral distribution of the facies; (2) to establish the sequence stratigraphic framework of the studied succession, based on the identification of key bounding surfaces and on the observable

distribution of facies; (3) to reconstruct the palaeogeographic and palaeoenvironmental evolution of the Oliete Subbasin during the Aptian, and (4) to discuss the palaeoenvironmental constraints controlling the observed distribution of benthic fauna in the Oliete Subbasin during the Aptian.

2 Geological setting

The Maestrazgo Basin was an intracratonic basin developed in Eastern Iberia during the latest Jurassic-Early Cretaceous reactivation of the Iberian Rift System, in a regional extensional regime related to the opening of the Western Tethys and North Atlantic oceans (*e.g.,* Martín-Chivelet et al., 2019; Aurell et al., 2019; Fig. 1A). The Oliete Subbasin, located at the northwestern margin of the Maestrazgo Basin, was tectonically active from the Barremian to mid Albian. Subsidence in this small sub-circular subbasin (c.30 km wide) was controlled by NW-SE-trending master faults and perpendicular NE-SW secondary faults, resulting in a sedimentary infill with marked thickness variability (Murat, 1983; Casas et al., 1997; Aurell et al., 2018; García-Penas et al., 2022).

The Oliete Subbasin was characterised by continental sedimentation during most of the Barremian, experiencing only occasional marine influence through an ephemeral narrow strait located in the south, connected to the shallow open seas of the adjacent Morella Subbasin (Aurell et al., 2018). During the latest Barremian and early Aptian, progressive transgression over the eastern areas of the Oliete Subbasin generated a wide seaway connecting both subbasins (García-Penas et al., 2022).

The Lower Cretaceous stratigraphic record of the subbasin is summarised in Fig. 1C. The Blesa Fm is a mixed carbonate-siliciclastic succession of highly variable thickness representing palustrine-lacustrine to restricted-marine environments (Aurell et al., 2018). The overlying Alacón, Josa and Oliete formations represent successive stages of marine sedimentation in the Oliete Subbasin (Canérot, 1972; Murat, 1983; García-Penas et al., 2022). This study focuses on

the Josa and Oliete fms, which represent two clearly discernible lithostratigraphic units. The early Aptian comprises clays, sandstones and sandy limestones deposited in various shallow-marine settings. This formation is 25 to 70 m thick, and spans the *D. forbesi* to *D. furcata* Tethyan ammonite biozones (Moreno-Bedmar, 2010; Sornay and Marin, 1972). The late Aptian Oliete Fm has a variable thickness of 45-100m and spans the *P. melchioris* to *A. nolani* biozones (Martínez et al., 1994; García et al., 2014). It encompasses a mixed carbonate-siliciclastic succession deposited in low energy marginal-marine settings. Overlying these two units, the latest syntectonic deposits of the Oliete Subbasin correspond to the estuarine-deltaic Escucha Fm (Pardo, 1979; Querol, 1990), which represents the definitive onset of continental deposition in the western Maestrazgo Basin during the early Cretaceous.

Material and methods

The Aptian mixed carbonate-siliciclastic deposits of the Josa and Oliete formations studied here have been logged in 11 bed-by-bed stratigraphic sections (Fig. 1C). The combination of these sections with field observations at 12 control points (Fig. 1C) has allowed the reconstruction of the thickness, facies distribution and sequence architecture of the studied units across the Oliete Subbasin. Logs and control points are distributed homogeneously across the Oliete Subbasin and its immediate surrounding areas, including the linking zones with the Morella and Las Parras subbasins (Fig. 1B). This new data set has been integrated with all available published data (e.g. Toulouse, 1971; Canérot, 1974; Canérot et al., 1982a, Canérot et al., 1982b; Marín et al., 1974; Samper et al., 1975; Ríos et al., 1978; Murat, 1983; Ruiz et al., 1985; Vennin and Soria, 1993; Soria et al., 1994; Soria, 1997; Vennin and Aurell, 2001; Peropadre, 2011) to produce a state-of-the-art sedimentological and sequence-stratigraphic framework.

The reported facies analysis is based on the microscope study of 173 polished slabs and 100 thin sections, complemented by field observations of architectural elements, textures, components and sedimentary structures. The correlation of the 11 sections presumes the

chronostratigraphic significance of several identified transgressive-regressive sequences *sensu* Johnson and Murphy (1984), which are bounded by prominent discontinuity surfaces that are traceable basinwide, as well as at outcrop scale.

Calcimetries were performed on 61 soft-sediment samples by specialized technicians of the Servicio de Apoyo a la Investigación (SAI) of the University of Zaragoza, using a mechanical manocalcimeter calibrated between sample batches using pure $CaCO_3$. The error of calibrated measurements averaged less than 5%.

Discussions on the distribution of the benthic fauna are based on taxonomic studies by Coquand (1865), Verneuil and De Lorière (1868), Mallada (1878), Bataller (1947), Toulouse (1971), Gómez-Alba (1998) and Ferratges et al. (2021), as well as on personal observations by the authors during ca. 40 field campaigns spanning the years 2019-2023. Relative abundances of components (Fig. 14) are based on visual estimations in outcrops, polished slabs and thin sections.

3 Updated lithostratigraphy: the Josa Formation

This work presents a revised lithostratigraphic framework for the Aptian record of the Oliete Subbasin, including the formal definition of the Josa Formation. Moreover, the lower boundary of the overlying Oliete Formation is also revised here. A summary of the key stratigraphic, sedimentological and palaeontological features of this newly defined unit across the Oliete subbasin is presented in Table 1.

The newly defined Josa Fm consists of a thickening- and shallowing-upward terrigenous succession, with a clay-dominated lower interval, and an upper interval composed of ochre, poorly to well lithified sandstones and bioclastic sandy limestones. These two lithological intervals were previously assigned to the Forcall Fm and to the lower member of the overlying Oliete Fm, respectively (e.g.. Canérot et al., 1982; Murat, 1983; Vennin et al., 1993; Soria et al.,

149 1995). However, the boundary between these two units was gradual, diachronous, and never
150 adequately defined, an issue that is solved here by considering the lower member of the Oliete
151 Fm (see Cabezo Negro Member in Canérot et al., 1982) as part of the newly defined Josa Fm.
152 This formation has clearly mappable lower and upper boundaries that correspond to
153 widespread, basin-scale unconformities associated to major lithological changes. Accordingly,
154 the definition of the Josa Fm follows the guidelines of the *International Stratigraphic Guide*,
155 which indicates that stratigraphic sequences bounded by regional unconformities should be
156 mapped as separate lithostratigraphic units (Murphy and Salvador, 1999).

157 It is also noted that the Forcall Fm around its type locality in the more open-marine Morella
158 Subbasin (Fig. 1B) is a marl-dominated unit with abundant and diverse open-marine fauna
159 (ammonites, brachiopods, echinoids, orbitolinids) and three well differentiated members
160 (Canérot et al., 1982). These members are not discernible in the Oliete Subbasin, where the
161 dominant terrigenous lithology of the Josa Fm reflects a proximal setting with significant
162 terrigenous influence.

163 ## 4 Facies analysis

164 The Aptian marine deposits of the Oliete Subbasin consists of two distinct unconformity-
165 bounded units, the Josa and Oliete formations, each characterized by specific facies and facies
166 associations representative of diverse shallow-marine to peritidal environments. Detailed
167 information of each individual lithofacies can be found in Table 2. A description of the facies and
168 facies associations followed by their interpretation is presented below.

169 ### 4.1 Josa Formation

170 #### 4.1.1 Offshore-prodelta facies association (FA1)

171 **Description:** FA1 is characterised by meter-thick massive marl and clay intervals (facies 1 and 2)
172 with millimetric silt intercalations (Fig. 2A), bioclastic wackestones with echinoderm fragments

and diverse benthic foraminifera (facies 12), orbitolinid floatstones (facies 9) and dm- to m-thick levels of massive to cross-laminated, fine, well-sorted, micaceous sandstone. Decimeter-thick interbeds of fine quartz sandstones with hummocky cross-lamination (Facies 4) appear occasionally among facies 1 and 2 (Figs. 2B, 3).

The terrigenous fine-grained facies 1 and 2 form m-thick tabular beds with mm-thick silt interbeds. Cm-thick Interbeds of fine sandstone with hummocky cross-lamination are also common. Beds of facies 1 and 2 yield complete echinoids, solitary corals, small thin-shelled pectinids and oysters, small gastropods, brachiopods, and diverse associations of decapod crustaceans (Ferratges et al., 2021), which locally occur in carbonate concretions (García-Penas et al., 2023). Bivalves, gastropods and solitary corals commonly occur as very small, "dwarf" morphotypes. Bryozoans and teeth of durophagous fish are locally abundant. The lowermost beds preserve a rich ammonite fauna dominated by roloboceratids (Moreno et al., 2007, 2010).

Orbitolinid floatstones (Facies 9) are intercalated in the clays forming isolated levels with gradual lower and upper boundaries. The skeletal components include abundant medium-sized (average diameter 3 mm), and well-preserved flat discoidal forms of *Palorbitolina lenticularis* embedded in a wackestone matrix also containing calcispheres, scarce lituolids, ostracods and rounded fragments of bivalves, gastropods and echinoderms, locally small solitary corals (Fig. 2C), as well as abundant very fine to fine quartz sand (Fig. 4E).

Occasionally, decimeter-thick beds of massive, well-sorted, fine-grained quartz sandstones with abundant muscovite and black organic debris (Facies 3, Fig. 4A) appear intercalated among mudstones (Facies 1) in depocentral areas of the subbasin (e.g., Alacón, Ariño, Fig. 5A). At Barranco del Moro, this facies forms amalgamated lobe-shaped beds containing disarticulated pholadomyid bivalves. Some levels present faint trough cross-lamination

Interpretation: Clay and marl beds with silty and orbitolinid-rich interbeds (Facies 1, 2 and 9) are interpreted to represent deposition in a low-energy offshore environment, mostly below wave

base, as evidenced by their lithology and the well-preserved open marine fauna they contain. Still, this environment is supposed to be relatively proximal, as suggested by the common interbeds of hummocky cross-stratified sandstones, which evidence a certain degree of storm influence. The predominance of roloboceratid ammonites has also been proposed as a proxy for proximality (Moreno et al., 2007), as they inhabited shallower environments than deshayesitids. The common occurrence of dwarf morphotypes of molluscs and corals could be evidence of a certain degree of environmental restriction (Pemberton et al., 1992; Flügel, 2010).

Beds of well-sorted massive sandstones with organic debris are interpreted as hyperpycnal flow deposits. Sediment-laden freshwater flows can become denser than marine water, plunging near the river mouth and generating a bottom current which can travel long distances basinward (Mulder and Alexander, 2001). As flow speed decreases with distance, the suspended sediment load falls to the bottom. Although this process can result in a variety of geometries and sedimentary structures (Shanmugam, 2018), massive well-sorted sand sheets, usually lacking bioturbation and with small organic debris dragged from the continent, constitute typical hyperpycnal flow deposits (Zavala et al., 2012; Zavala, 2020). Thus, hyperpycnal flow deposition is thought to be the primary origin of these sandstone beds, although the occasional presence of faint trough cross-lamination at some localities (e.g. Barranco del Moro) could indicate storm influence.

4.1.2 Delta front facies association (FA2)

Description:FA2 is composed of well-sorted fine-grained massive sandstones lacking bioturbation or sedimentary structures (Facies 3), which grade upwards into fine bioclastic sandstones containing large endobenthic bivalves (Facies 5), and then into upwards-coarsening fine to microconglomeratic sandstones with trough cross-stratification (Facies 6a) containing rounded, well-sorted fragments of serpulids, oysters and other molluscs (Fig. 4B), as well as ostracods and very rare charophyte gyrogonites.

Massive sandstones (Facies 3) form m-thick beds composed of fine quartz sand with abundant muscovite, as well as black organic debris. In general, beds of Facies 3 in this association are thicker and coarser-grained than their counterparts of the underlying offshore FA1.

Bioclastic sandstones (Facies 5) usually form dm to m-thick tabular beds with a fine matrix of quartz sand and muscovite, with a significant bioclastic fraction composed of fragments of oysters, trigoniids, other undetermined bivalves, and gastropods (Fig. 4C). These beds contain well-preserved disarticulated shells of large endobenthic bivalves, most commonly abundant and diverse trigoniids, as well as oysters, occasional carditids and venerids, as well as abundant cassiopid and turritellid gastropods and scarce brachiopods (Table 2). The large mollusc shells are interpreted to be parautochtonous, as they are mostly disarticulated but not rounded off or broken. Bioturbation is minimal, and the only common microfaunal elements are ostracods and scarce rounded orbitolinids.

Coarse cross-stratified sandstones (Facies 6a) form m-thick coarsening-upwards beds. Locally (Obón), the uppermost part of these beds is microconglomeratic, containing mm-sized rounded quartz grains. Bioturbation is minimal and composed only of *Skolithos* isp. and *Ophiomorpha* isp.

Interpretation:FA2 is interpreted to represent a coarsening-upward delta succession with a certain degree of wave influence (Bhattacharya and Waker, 1992; Bhattacharya and Giosan, 2003).

As in FA1, beds of Facies 3 are interpreted to represent hyperpycnites (Zavala, 2020). In FA2, however, these beds are thicker and coarser-grained than in FA1 and are interpreted to have been deposited in a more proximal setting in the delta front-prodelta transition. This is also supported by their close association to fine-grained offshore (i.e. prodelta) facies 1 and 2.

Bioclastic sandstones with large molluscs (Facies 5) represent deposition in the distal part of the delta front. This environment would have been generally quiet, as indicated by the generally good preservation of the shells, but would have been subjected to episodic high-energy events

248 (i.e. storms), leading to disarticulation. The well-sorted and rounded bioclastic matrix probably
249 represents a mixture of parautochthonous and allochthonous elements. We interpret the
250 increasingly high amounts of quartz sand and coarsening-upward trend locally observable in this
251 facies as a result of the progradation of the delta system. The low diversity of the trace fossil
252 and microfaunal assemblages could be attributed to rapid variations in environmental
253 conditions, which are to be expected in a delta front environment due to the proximity of
254 freshwater sources (e.g., Hansen and MacEachern, 2007; Veiga et al., 2013).

255 The relatively coarse, trough cross-stratified sandstones (Facies 6a) with scarce and low-diversity
256 ichnofacies and almost no microfauna are interpreted as very shallow upper shoreface deposits
257 of a delta system heavily influenced by terrestrial supply (Pemberton et al., 2012; Veiga et al.,
258 2013).

259 #### 4.1.3 Carbonate littoral facies association (FA3)

260 **Description:**FA3 includes bioclastic wackestones to packstones (facies 13) and cortoidal
261 packstones-grainstones with abundant green algae fragments (facies 14). Both facies present
262 variable small amounts of quartz sand. This FA is very localized, only occurring in the uppermost
263 part of the Josa Fm in Estercuel (Fig. 6).

264 Bioclastic W-P form tabular beds (Facies 13). Other faunal components include diverse benthic
265 foraminifera (Table 2), as well as debris of bivalves, gastropods, echinoderms, ostracods and
266 green algae. Facies 14 form tabular beds with a nodulose appearance due to intense
267 *Thalassinoides* bioturbation. Decapod remains are very abundant and are occasionally
268 associated with burrows. Grain associations are dominated by cortoids with destructive
269 coatings. A variety of bioclasts form the cortoid cores, including mollusc, echinoderm and
270 serpulid remains. Green algae fragments are abundant. Microfaunal associations are dominated
271 by textulariid foraminifera, mainly *Choffatella*.

Interpretation: Facies 13 is interpreted to represent deposition in a shallow, low-energy carbonate environment with a relatively low degree of environmental stress, as evidenced by the relatively high faunal diversity. Facies 14 was probably deposited in a shallower marginal subtidal area, as grain associations with abundant cortoids and green algae are typical of very shallow euphotic environments (e.g., Flügel, 2010). The predominance of agglutinated foraminifera in Facies 14 could suggest increased environmental stress levels, as low-diversity microfaunal assemblages composed mostly of textulariids have been related to reduced salinity, alkalinity or oxygen levels (Haynes, 1981; Flügel, 2010; Barroso-Barcenilla et al., 2011).

It is interesting to note the relatively small amounts of quartz sand in FA3, despite the proximity of Estercuel to Josa and Obón, which were areas dominated by terrigenous sedimentation. Longshore currents in the Oliete Subbasin are interpreted to have been weak, due to its geometry and bathymetry (García-Penas et al., 2022). Moreover, in deltaic settings where the fluvial currents are relatively strong, the fluvial jet can interfere with these weak longshore currents, acting as a hydraulic barrier (Anthony, 2015). Furthermore, the growing deltaic prism in the Josa-Obón area may have acted as a morphodynamic groyne (sensu Ashton and Giosan, 2011), deflecting longshore currents and effectively shielding the southwestern margin of the subbasin, allowing for the development of a marginal environment dominated by carbonate sedimentation in Estercuel.

4.1.4 Mixed dunes facies association (FA4)

DescriptionFA4 is composed of tabular sandy bioclastic packstone and grainstone (Facies 7) beds with simple sets of large-scale planar cross-stratification dipping to the SE and NNE (Fig. 7A). Individual beds reach a maximum thickness of 1.7 m and a lateral extension in the order of 100-200 m, and are bounded by master surfaces subparallel to stratification, which are associated to bivalve shell beds composed of tightly packed, mostly articulated bivalves oriented randomly in the upper part of each cross-bedded bed.

297 **Interpretation:**These cross-bedded deposits are clustered in the north-western area of the
298 Oliete Subbasin (Figs. 6, 8). Following the decompaction algorithms for grain-supported
299 sediments of Goldhammer (1997), a minimum original thickness of ca. 2 m can be inferred for
300 individual cross-stratified bodies in Alacón, suggesting that these bedforms were generated in
301 minimum water depths of ca. 10 m (decompacted dune height represents roughly 17-40% of
302 the total water depth: Dalrymple and Rhodes, 1995; Olariu et al., 2012).

303 The high degree of articulation of the bivalve accumulations associated to each cross-bedded
304 body contrasts with the high-energy conditions necessary to produce large scale bedforms. The
305 tight packing, high degree of articulation and good preservation of the shells resemble those of
306 time-averaged biogenic concentrations generated during sediment-starved stages in shallow-
307 marine settings (Kidwell, 1993; Kumar et al., 2009), which would imply relatively prolonged
308 periods of inactivity.

309 According to these characteristics, we interpret these cross-stratified bodies as subtidal dunes
310 (Olariu et al., 2012) generated during large-scale storm events. The bimodal perpendicular
311 palaeocurrent pattern fits the longshore and cross-shore currents of large storms (Walker, 1984;
312 Bádenas and Aurell, 2001). Periods of dune inactivity between large storm events would allow
313 the colonization of dunes by burrowing bivalves. This interpretation is also consistent with the
314 hummocky bedding observable in laterally equivalent beds in nearby areas (Fig. 2L).
315 Furthermore, the observed storm wave patterns in present-day shallow enclosed basins with
316 similar geometry to the Oliete Subbasin show that maximum wave height and energy tend to
317 develop in the central, deeper parts of the basin (Hesser et al., 2013), fitting the distribution of
318 dunes in the Josa Formation.

319 #### 4.1.5 Siliciclastic-bioclastic littoral facies association (FA5)

320 **Description:**FA5 predominates at the western margin of the subbasin (Josa, Obón). It includes
321 well-lithified bioclastic sandstones (Facies 6a), some of them cross-bedded and with rare

Ophiomorpha and *Skolithos* isp. burrows, and bioclastic packstones and grainstones (Facies 12) with fragments of oysters, thick, and thin-shelled bivalves, ostracods, scarce echinoderms, agglutinated foraminifera (mainly *Choffatella*) and variable amounts of quartz sand. Most bioclasts are fragmented and rounded.

Interpretation: This facies association is interpreted as deposited in a winnowed mixed carbonate-siliciclastic shoreface subject to wave or current action, as evidenced by the exclusive presence of the *Skolithos* ichnofacies (Pollard et al., 1993; Pemberton et al., 1992, 2012). This is also supported by the presence of coated grains (Flügel, 2010), although these are not abundant and could have been derived from nearby environments.

4.1.6 Siliciclastic coastal plain facies association (FA6)

DescriptionFA6 is found in the uppermost part of the Josa Fm in the northwest of the subbasin (Blesa) (Fig. 8B). It comprises poorly exposed clay-dominated intervals with intercalations of channelised bioclastic sandstones (Facies 6b). The covered intervals preserve abundant wood fragments. Facies 6b presents abundant rounded bioclasts of small oysters and other bivalves.

Interpretation:This association is interpreted to represent a low-energy peritidal environment, possibly a mud-dominated coastal plain dissected by small tidal gullies (e.g., Dalrymple, 2010). However, no detailed assertions can be made about this depositional environment due to the poor outcrop conditions.

4.2 Oliete Formation

4.2.1 Protected lagoon facies association (FA7)

Description:FA7 is characterised by beds of grey clays with scarce pyritized moulds of tiny (<2mm) bivalves and gastropods (Facies 1) associated with mud-supported floatstones of articulated bivalves and gastropods (facies 10), alternating with disarticulated and fragmented oyster floatstones and rudstones (facies 11 a and 11b). Occasionally, facies 10 and 11 grade

upwards into dm-thick beds of bioclastic packstones and grainstones (F12) with variable amounts of quartz sand. This facies association forms the bulk of the Oliete Formation across the Oliete Subbasin (Figs. 9, 10)

Facies 10 is composed of loosely to tightly packed accumulations of internal moulds of bivalves and gastropods embedded in a white mudstone to wackestone matrix (Figs. 2D, 4E). The matrix contains varying amounts of small bioclasts, fine quartz sand and occasional rip-up clasts. The bivalve associations include a variety of filter-feeding groups adapted to different modes of life, with deep infaunal taxa (pholadomyids, hiatellids, lucinids), shallow infaunal taxa (venerids, arcticids and carditids), epibyssates (limids) and abundant epifaunal oysters such as *Crassostrea.* Turritellid and large cassiopid gastropods are common. Other gastropod groups (cerithiids, nerineids) appear occasionally. Colonies of serpulids mollusclocally co-occur with mollusc accumulations. Other groups, such as echinoderms and green algae are rare and represented by disarticulated and broken bioclasts. Microfauna is scarce and includes low-diversity associations of ostracods and agglutinated foraminifera (Table 2). At the northeastern margin of the subbasin (Ariño, Fig. 1C), some bivalve moulds are colonized by patelliform mollusces (i.e “limpets” s.l.) (Fig. 2E).

Facies 11 consists of dm to m-thick beds of oyster floatstones and rudstones. Across most of the subbasin, these beds are composed of gryphaeids and ostreids, including the genus *Crassostrea* (facies 11b). Shells are mostly disarticulated but well preserved. Matrix is scarce to completely absent, and some beds exhibit low-angle planar cross-stratification. At the northern margin of the subbasin (Cabezo Negro), this facies contains large articulated ostreids (facies 11a) associated with in-situ serpulid buildups, forming floatstone beds with a micritic matrix (Facies 11a, Fig. 2F).

Facies 12 consists of dm-thick beds of packstones and grainstones containing bioclasts of bivalves, gastropods, serpulids, echinoderms, and scarce brachiopods, as well as variable but

small quantities of cortoids and fine quartz sand. The microfauna is composed only of ostracods and agglutinated foraminifera. Some beds contain accumulations of monaxon sponge spicules, often associated with crustacean microcoprolites and micritic flat rip-up clasts (Fig. 4F). Some beds show a clear fining-upward trend and convex-down orientation of bivalve shells. Faint cross-lamination is common.

Interpretation: Facies 10 is interpreted to represent primary biogenic concentrations sensu Fürsich and Oschmann (1993), deposited in a quiet lagoonal environment protected from current and wave action, allowing for the preservation of in-situ or parautochtonous accumulations of benthic filter-feeding bivalve communities. Matrix-supported limestones containing low-diversity microfaunal associations dominated by agglutinated foraminifera and ostracods, crustacean microcoprolites and detrital quartz are indeed common deposits in shallow and low-energy stressed environments (Zinke et al., 2005; Flügel, 2010; Brandano et al., 2015; Dalvand et al., 2015; Bádenas et al., 2018). It is unclear whether patelliform gastropods colonized reworked bivalve moulds or whether they were attached to the outer part of the alive bivalve and were compressed on the moulds after dissolution of the shells during diagenesis. In any case, the association of bivalves and patelliform molluscs would seem to indicate a very shallow-water origin for the bivalve accumulations, as most limpet groups inhabit shallow subtidal to intertidal environments (Nakano and Sasaki, 2011). Slow water circulation in the lagoon probably favoured salinity oscillations, thus inhibiting the development of diverse microbenthic communities and of stenohaline organisms such as cephalopods, corals and bryozoans. Other stressors resulting from restricted circulation (e.g. bottom hypoxia) could have also conditioned the benthic faunal associations (Witzke, 1987). The existence of unfavourable conditions at the sediment-water interface is supported by the exclusive presence of articulated specimens of two small (1 mm) morphotypes of a bivalve and a gastropod in the clay beds (Facies 1), which dominate in sequence O1 in the depocentral areas of Alacón and Cabezo Negro (Figs. 1, 5, 10).

The winnowed accumulations of disarticulated but mostly well-preserved oysters observed in Facies 11b are typical of Storm-wave skeletal concentrations (sensu Fürsich and Oschmann, 1993). These beds are interpreted to have developed in very shallow environments with lowered or oscillating salinity, subject to episodic wave or current energy. Energy levels were high enough to winnow away fine sediment and bioclasts, but not enough to transport and damage the heavy oyster shells. We interpret these accumulations as marginal parautochthonous oyster biostromes reworked by storm wave action. These biostromes probably developed in the nearshore subtidal areas of the bay, while in-situ bivalve accumulations (Facies 10) represent a lower-energy lateral equivalent deposited in quieter areas, where favourable environmental conditions fostered a more diverse benthic community. Facies 11a represents the low-energy equivalent of facies 11b, probably developed in areas protected from direct storm influence.

Facies 12 represent bioclastic deposits developed in the marginal areas of the lagoon under common storm influence, as indicated by the restricted bioclastic fraction, fining-upwards trend, convex-down orientation of bivalve shells, occasional cross-lamination and general fragmentation and good sorting of the grains (Aigner, 1985; Flügel, 2010). Thin beds of facies 12 intercalated between thick packages of facies 10 and 11 are interpreted as tempestitic deposits.

4.2.2 Low-energy peritidal facies association (FA8)

Description: At the southern margin of the subbasin (Estercuel), FA8 is composed of tabular dark grey clay beds (Facies 2) which are mostly azoic, except for occasional monotypic accumulations of ostracods and in-situ aggregations of *Crassostrea* (Fig. 2G). The clay beds contain interbeds of oyster floatstones and rudstones (Facies 11a) and mollusc floatstones (Facies 10) containing trigoniids and other bivalves (see Table 2) in a bioclastic matrix.

At the northern margin of the subbasin (Blesa), FA8 is dominated by alternations of floatstones of large articulated ostreids (Facies 11a) associated to mollusc floatstones (Facies 10) containing

bed-specific faunal associations composed either of turritellid and cassiopid gastropods (Fig. 2H) or venerid bivalves.

Interpretation: The exclusive presence of *Crassostrea* oyster aggregations and of ostracod accumulations in the grey clays strongly suggests that facies 2 represents sedimentation in a high-stress nearshore environment, possibly a mudflat (Stenzel, 1971; Allmon, 1988, 2011; Komatsu et al., 2002; Flügel, 2010; Waite and Allmon, 2016). This is supported by the depositional continuity of facies 2 with beds of facies 10 and 11, which reflects a lateral relationship with the protected lagoon FA7.

The faunal associations found in Blesa also suggest deposition in a low-energy stressed peritidal environment colonized episodically by opportunistic taxa (e.g., Flügel, 2010; Cuitino et al., 2014; Abdelhady et al., 2020), possibly a carbonate mudflat.

4.2.3 Siliciclastic tidal flat facies association (FA9)

Description: FA9 appears in the upper part of the Oliete Fm in the central and NW areas of the Oliete Subbasin (Alcaine, Blesa). It comprises well-sorted fine sandstone beds with planar cross-stratification (Facies 6a), overlain by poorly lithified sandstone beds with heterolithic and ripple cross-lamination (Facies 8, Fig. 2J, K, N) and dm-thick intercalations of channelised sandstone with trough cross-lamination (Facies 6b) (Figs. 9J, K, N). This association is mostly azoic, except for abundant oysters and occasional trigoniids in the lower beds of cross-stratified Facies 6a.

Interpretation: This association represents deposition in a siliciclastic tidal flat. The mollusc-bearing cross-stratified sandstones (Facies 6a) are interpreted as very proximal subtidal sand bars. The unfossiliferous heterolithic sands and silts (Facies 8) represent deposition in a highly stressed intertidal-supratidal sandflat environment, crossed by small tidal channels (Facies 6b).

4.2.4 Iron ooid-bearing facies association (FA10)

Description: FA10 corresponds to a single horizon of bioclastic-cortoidal packstones-grainstones with variable proportions of iron ooids (Facies 16) (Fig. 4K), which can be correlated across the western margin of the Oliete Subbasin. The thickness of the iron ooid-bearing interval, as well as the amount of ooids in the bioclastic matrix, reach a maximum near Josa and Alcaine, decreasing rapidly to the northeast. In Alacón, ooids are rare. In this facies, bioclasts are broken and rounded, and include fragments of oysters, recrystallised fragments of bivalves, gastropods, scarce echinoderms, ostracods and rare lituolid foraminifera. Many bioclasts present cortoidal micrite coatings. Iron ooids are poorly sorted, and range in size from 0.2 to 1.3 mm. Most of them exhibit thin ferruginous coatings surrounding a nucleus which can be either an amorphous ferruginous particle or a fragment of a broken ooid. The nucleus to coating-thickness ratio is high.

Near Alcaine, this facies forms lobate cross-stratified bodies (up to 3.5 m-thick and 100s of metres of extent) (Fig. 7B), which pinch out laterally into mollusc floatstones/rudstones (Facies 10 and 11) of the Protected Lagoon FA7. The lobes exhibit large-scale cross-stratification dipping to the SE. These beds have a dominant packstone texture, although some samples present bands or patches of matrix-less grainstone. The grains consist of a mixture of iron ooids (with increasing-upward proportion) and broken bioclasts of oysters, thin-shelled bivalves, small gastropods, rare echinoderms and serpulids, as well as articulated and well-preserved ostracods, gastropods, small bivalves, and whole serpulid colonies. The well-preserved fauna is probably parautochthonous and only underwent very short transport, while the bioclasts and iron ooids are probably resedimented.

Interpretation: The packstone to grainstone texture and abundance of micritic coatings in Facies 16 suggest constant agitation in a shallow, well oxygenated, and euphotic environment (Flügel, 2010). The lobe-shaped beds in Alcaine are interpreted as storm lobes deposited around the storm wave-base by episodic unidirectional currents flowing towards the deeper parts of the

bay (i.e. cross-shore return currents of major storms). A storm origin is supported by the presence of well-preserved but resedimented fauna and and the packstone-grainstone texture alternations, indicating episodic energy variations. The well-preserved fauna corresponds to parautochthonous elements of the Protected Lagoon FA (facies 10 and 11), while the bioclastic fraction was probably resedimented from coastal bioclastic belts (facies 12).

The features of the iron ooids coincide with Type 1 ooids of Reolid et al. (2008), which the authors interpret to have been generated in iron-rich paleosols developed in a coastal plain environment following subaerial exposure of the sea floor. Similar ooids with an analogous interpretation have also been described in lateritic deposits of the lower Barremian Blesa Formation in the Oliete Subbasin, generated under intense chemical weathering during warm and humid climate conditions (Laita et al., 2020). Thus, we interpret that the iron ooids were probably sourced from laterite-like paleosols developed on exposed areas around the Oliete Subbasin, and resedimented in very proximal storm-influenced marine environments.

4.2.5 Open lagoon facies association (FA11)

Description: FA11 appears only in the uppermost part of the Oliete Formation (Fig. 9, 10). It comprises peloidal-bioclastic and cortoidal grainstones (facies 13 and 14), which locally form cross-bedded beds (Facies 15, Figs. 4J, 8E), as well as bioclastic packstones and grainstones containing abundant remains of oysters and other thick-shelled bivalves (facies 12).

Facies 13 and 14 contain peloids, cortoids, remains of thin-shelled bivalves, gastropods, echinoids, ostracods, green algae, and variable amounts of fine quartz sand. Benthic foraminifera are diverse and relatively abundant, and include several morphotypes of very small unidentified uniseriate, biseriate and coiled forms, occasional miliolids, *Lenticulina*, *Choffatella* and orbitolinids, including *Mesorbitolina texana*. Fragments of decapods are also abundant. In Alcaine and Cabezo Negro, these facies enhibit planar cross-bedding dipping to the SSE (Figs. 9,

10). Glauconite appears in variable amounts in FA11, locally forming massive accumulations (Fig. 11G) associated to pervasive *Thalassinoides* bioturbation (Fig. 11F) and oyster remains.

Interpretation: According to the abundance of cortoidal-peloidal facies with shallow-marine fauna, FA11 is interpreted to have been deposited in a low to moderately energetic shallow subtidal environment in the euphotic zone with normal marine salinity, possibly an open lagoon (e.g., Bachmann and Hirsch, 2006; Flügel, 2010; Wilmsen et al., 2010).

Regarding the observed glauconite accumulations, authigenesis of glauconite was common in shallow marine environments during the Cretaceous (e.g., Banerjee at al., 2016; Bansal et al., 2020, 2023; Jafarzadeh et al., 2020), including in terrigenous coastal environments (e.g., Geptner and Ivanovskaya, 2000) and protected lagoons (El Albani et al., 2005). It has been suggested that glauconite authigenesis in nearshore environments was linked to the prevailing climate during the Cretaceous (Bansal et al., 2022). The general warm-and-wet greenhouse conditions (Hay and Floegel, 2012, Föllmi, 2012, Huck and Heimhofer, 2021), with intense rainfall and extensive development of wetland biomes (Hay et al., 2019) promoted intense chemical weathering of exposed reliefs. In turn, intense runoff laden with detritals would have increased the Fe, Si, Al and K content of nearshore waters. This water composition coupled with hypoxic reducing conditions, due to either restricted water circulation or high nutrient inputs, created a prime environment for the precipitation of glauconite (McConchie et al., 1978; Harder, 1980; Bansal et al., 2023). Authigenesis was especially fast and intense in depositional environments with optimal substrates for nucleation, such as fecal pellets and small bioclasts (Hower, 1961; Banerjee et al., 2016; Chakrabarty et al., 2022).

5 Facies evolution and sequential architecture

The analysis of the overall distribution of the facies associations across the Oliete Subbasin, coupled with the identification and correlation of major discontinuity surfaces, has resulted in

518 the proposal of a sequence stratigraphic framework for the Aptian seimentary succession of the
519 Oliete Subbasin.

520 Four unconformity-bounded sequences are recognised (Figs. 3, 4). The identified sequences
521 follow the transgressive-regressive (T-R) sequence model sensu Johnson and Murphy (1984),
522 which has proven to be useful in shallow marine areas where strata typically do not form
523 systems-tracts and maximum regressive surfaces tend to be easily recognizable (Catuneanu,
524 2009). The Josa Formation includes a single long-term T-R cycle (Sequence J), whereas the Oliete
525 Formation includes three T-R sequences: O1, O2 and O3. The four sequences have variable
526 thicknesses, ranging from 6 to 57 meters. The facies architecture of each sequence, and the
527 description of their key bounding surfaces is presented below.

528 **5.1 Sequence J**

529 Sequence J represents a third-order transgressive-regressive cycle spanning ca. 1.3 Ma (Moreno-
530 Bedmar et al., 2010; Gale et al., 2020). The onset of the sedimentation of sequence J is marked
531 by a major transgressive surface overlying the Alacón Fm (discontinuity B1 in Fig. 3, equivalent
532 to discontinuity D5 in García-Penas et al., 2022). This surface represents an abrupt lithological
533 shift from the cross-stratified proximal tidal dune deposits topping the underlying Alacón Fm to
534 the offshore marls and clays of the lower Josa Fm. The surface presents a well-developed
535 hardground (Fig. 11A) and abundant *Gastrochaenolites* isp. and *Trypanites* isp. borings, as well
536 as encrusting oysters. In marginal areas of the subbasin (e.g., Blesa, Fig 1C), this surface shows
537 prominent palaeokarst features developed during a period of subaerial exposure, which were
538 encrusted by oysters during the subsequent transgressive event (Fig. 11A, B). This discontinuity
539 is associated to a stratigraphic gap of uncertain duration spanning part of the *D. oglanlensis* and
540 *D. forbesi* ammonite biozones (Moreno-Bedmar et al., 2010; García-Penas et al., 2022).

541 The facies evolution of the Josa Formation shows a very asymmetrical T-R cycle (Fig. 3). A
542 calcareous condensation bed containing abundant ammonites (Moreno-Bedmar et al., 2010),

543 located within the first metre of the sequence (Fig. 3) is interpreted to represent the maximum
544 flooding zone of the sequence. Above this bed, the long-term shallowing-upwards trend of
545 sequence J is coupled with an upward decrease in $CaCO_3$ content in the marl and clay dominated
546 intervals of FA1 (Fig. 3) $CaCO_3$ values reach a minimum around an orbitolinid floatstone bed
547 (Facies 9) which can be recognised subbasin-wide (Fig. 3, 6). A progressive shallowing-upward
548 trend is also evidenced by the progressive basinwide appearance of coarser-grained littoral sand
549 dunes (FA4). A discontinuity surface, which is traceable basinwide (discontinuity B1.1, Fig. 3,
550 11C, 12A), overlies these facies. This discontinuity is in turn overlain by FA1 across the subbasin,
551 indicating a short-lived deepening stage. The uppermost part of the Josa Formation is
552 characterized by the reappearance basinwide of littoral environments, including well-developed
553 deltaic successions (FA2, Fig. 12A), littoral sand dunes (FA4) and siliciclastic tidal flats (FA5).

554 Sequence J is topped by a large-scale discontinuity surface recognizable basinwide (discontinuity
555 B2, Fig. 3). In the depocentral areas of the Oliete Subbasin (e.g., Alacón) this discontinuity is
556 expressed as a sharp, slightly erosional, iron-stained surface (Fig. 13E). In more marginal settings
557 this surface is clearly erosional and incises the cross-bedded bioclastic sandstones at the top of
558 sequence J (Fig. 13A, B). Near Oliete, the discontinuity contains abundant *Trypanites* borings
559 (Fig. 13C). Pervasive *Thalassinoides* isp. burrows are locally associated with the beds
560 immediately underlying this surface (Fig. 11D). Discontinuity B2 also involves an abrupt facies
561 change from the mixed carbonate-siliciclastic cross-bedded packstones and grainstones of the
562 uppermost Josa Formation to the bivalve-oyster floatstones and rudstones of the lower Oliete
563 Formation.

564 **5.2 Sequence O1**

565 The overall facies evolution of Sequence O1 has been interpreted as an asymmetrical T-R cycle
566 (Fig. 9) with a condensed transgressive hemicycle. The sequence has an estimated duration in
567 the range of third-order sequences (Fig. 1C, García et al., 2014; Gale et al., 2020). In Alacón and

568 Josa, the condensed transgressive interval of Sequence O1 consists of a dm-thick iron-stained
569 shell bed (Fig. 13A, B, D) with two clearly defined intervals; a lower interval containing mudstone
570 intraclasts, abundant quartz sand and reworked and poorly preserved shell debris, and an upper
571 carbonate-dominated interval composed of whole and fragmented shells of large bivalves, small
572 phosphate nodules and in-situ accumulations of encrusting serpulids (Fig. 13F, G). The size and
573 degree of preservation of the shells increases upwards, as do the intensity of iron staining and
574 the amount of phosphate nodules (Fig. 13D, F). This layer is interpreted as a composite shell bed
575 (Kondo et al., 1998; Zecchin et al., 2017). The lower interval represents a transgressive lag
576 containing poorly preserved bioclasts and calcareous intraclasts reworked during transgressive
577 ravinement of the underlying deposits. Ravinement is evidenced by the erosional nature of the
578 underlying discontinuity surface, which incises the uppermost deposits of Sequence J (Fig. 13A,
579 E). The upper portion of the shell bed is interpreted as an onlap shell bed (Zecchin et al., 2019),
580 generated during a stage of intense sediment starvation or bypass, in which the deposit
581 underwent early cementation and iron staining, becoming an ideal substrate for encrusting taxa.
582 The upwards increase in the degree of preservation of the bivalve shells can be explained by a
583 progressive reduction in environmental energy due to gradual deepening as transgression
584 progressed (Zecchin et al., 2019).

585 The upper boundary of this condensed bed is intensely iron-stained and is interpreted to
586 represent the maximum flooding surface of the sequence (Fig. 9, 13D). Discontinuity B2 is also
587 locally characterised by a well-developed ferruginous crust located below the basal
588 transgressive shell-bed of sequence O1 (Fig. 13B), suggesting that the transgressive stage of
589 sequence O1 was a complex multi-stage process probably composed of multiple alternating
590 stages of sedimentation and starvation or bypass. In other areas of the subbasin where the
591 composite shell bed is not present, the transgressive hemicycle of the sequence is characterised
592 by dm-thick beds of mixed carbonate-siliciclastic Facies 5. The regressive hemicycle of the
593 sequence represents a gradual transition from the deeper facies of the protected lagoon FA7

(facies 10 and 11), which constitutes the bulk of the sequence across the basin, to proximal storm-influenced beds (facies 12), as well as the Low-Energy Peritidal FA8.

The upper boundary of Sequence O1 (discontinuity B3) presents different characteristics across the Oliete Subbasin. In the central and eastern areas of the subbasin (Fig 1C; Alacón, Alcaine, Josa, Montalbán), this discontinuity is associated with beds of bioclastic grainstones with abundant iron ooids and pisoids (FA10). These ooids are likely to be derived from paleosols formed at the margins of the Montalbán High (Fig. 8C) following subaerial exposure during the regressive stage of sequence O1. The iron ooids would have been reworked during the earliest stages of the subsequent transgressive event and redistributed across the western margin of the subbasin. The presence of iron ooids in the same stratigraphic interval south of the Montalbán High (Montalbán log, Fig. 1C) provides further evidence of this exposed area being the source of the ferruginous ooids.

In the northeastern sector (Fig. 1C; Cabezo Negro, Ariño, Barranco del Moro) the unconformity is expressed as a palaeokarst with a reddish infill (Fig. 11E). In the southern areas of the subbasin (Fig. 1C; Estercuel, Montalbán), poor outcrop conditions impede observation.

5.3 Sequence O2

Sequence O2 is mostly covered across most of the Oliete Subbasin, and its lateral facies distribution cannot be confidently reconstructed (Fig. 9). The sequence has an estimated duration in the range of third-order sequences (Fig. 1C, García et al., 2014; Gale et al., 2020). The description of the vertical facies evolution of this stratigraphic interval focuses on the depocenter of the subbasin (i.e. Alacón section), where Sequence O2 is well exposed and also presents a subdivision into four shallowing-upward subsequences bounded my minor discontinuities (Figs. 9, 10).

Most of subsequence 1 (SS1) is dominated by the protected lagoon FA7, with occasional cm-to dm-thick intercalations of bioclastic packstone interpreted as tempestites (Facies 12, Fig. 4G).

The uppermost part of the sequence is characterised by the appearance of coarsening-upwards beds of bioclastic packstones and grainstones with faint cm-scale planar cross-lamination (facies 12), topped by a bioturbated and iron-stained surface.

Subsequence 2 (SS2) exhibits a similar vertical facies evolution to SS1. The Protected Lagoon FA7 forms the bulk of the subsequence. The uppermost SS2 presents bioclastic beds of facies 12 with accumulations of recrystallised monaxon sponge spicules. These spicule accumulations are accompanied by ostracods, abundant crustacean microcoprolites and flat micritic rip-up clasts (Fig. 4F).

The bulk of subsequence 3 (SS3) is again dominated by the protected lagoon FA7. As in previous subsequences, the basal interval of SS3 is mostly covered with some exposed well lithfied bioclastic tempestites. Of special interest is a m-thick cross-bedded lobe-shaped tempestite bed set (Fig. 9) with an upwards-fining trend and preferentially convex-down oriented, well sorted disarticulated mm-scale bivalve shells. Some cross-beds of the set are true encrinites containing mostly partially articulated crinoid elements, as well as abundant well-preserved cassiduloid echinoids. The bed set is overlain by a m-thick packstone bed (facies 12) containing debris of echinoderms, small bivalves and gastropods, ostracods, serpulids and green algae, as well as small amounts of quartz sand. The latter bed has a lateral extension of several kilometres, and is therefore correlatable between outcrops, having also been recognised in Cabezo Negro and Alcaine (Fig. 10).

Subsequence 4 (SS4) contains a high proportion of quartz sand. Its lower part is composed of beds of facies 1o and 11 containing abraded and rounded oyster fragments bioeroded by *Entobia* isp., and well-preserved small gastropods. The upper part is composed of thick beds of facies 12 containing abundant cortoids and quartz sand with ripple cross-lamination.

The interpretation of Sequence O2 as a long-term T-R cycle is supported in Alacón by the predominance of low-energy lagoonal facies in the lower subsequences and the progressive

appearance of proximal facies with abundant detrital quartz towards the upper part of the sequence. In other areas of the Oliete Subbasin, where Sequence O2 is mostly covered, this shallowing-upward trend is still recognizable; in Blesa and Estercuel, peritidal facies (FA8, FA9) tend to dominate the upper part of the sequence (Figs. 8D, 9, 10).

The upper boundary of Sequence O2 (discontinuity B4) is locally erosional (Fig. 11F). In the northern and northwestern areas of the subbasin, discontinuity B4 is expressed as a transgressive surface marking a sharp transition from tidal flat deposits (Blesa, Fig. 1C) and very proximal subtidal cortoidal grainstones (Alacón, Fig. 1C) to protected lagoon facies (Fig. 9).

5.4 Sequence O3

The vertical facies evolution of sequence O3 cannot be confidently reconstructed due to poor outcrop exposure, but has been tentatively interpreted as an asymmetrical T-R cycle based on the observable vertical stacking of facies (Fig. 9). The sequence has an unknown duration and is thinner than sequences J-O2 (Fig. 12B), but is also estimated to be in the range of third-order sequences based on the available biostratigraphic data (Fig. 1C; García et al., 2014; Gale et al., 2020). The sequence is dominated by cortoidal and peloidal packstones-grainstones of the Open lagoon FA11, with local development of orbitolinid blooms (Fig. 9).

The basal interval of the sequence, immediately overlying discontinuity B4, displays massive glauconite accumulations. A very shallow-water origin for this glauconitic interval is supported by the association of glauconite with autochthonous and parautochthonous specimens of the intertidal oyster *Crassostrea*, high concentrations of *Thalassinoides* bioturbation (Fig. 11F), the local occurrence of ripple cross-lamination and the abundance of shallow-water bioclasts. In fact, the maximum concentrations of glauconite in Sequence O3 occur in low-energy intertidal facies with in-situ *Crassostrea* aggregations in Estercuel (Fig. 9).

The genesis of these glauconite accumulations may be related to the reworking of the siliciclastic peritidal deposits of the uppermost part of sequence O2 during the transgressive stage of

669 sequence O3, which could have loaded the sea water with the necessary cations for glauconite
670 authigenesis (Bansal et al., 2023), leading to massive and rapid precipitation in the peloidal and
671 fine bioclastic deposits that characterize Sequence O3. Precipitation could have been facilitated
672 by reducing dysoxic conditions in the bottom of the lagoon, caused by low rates of water
673 circulation.

674 The upper boundary of Sequence O3 (discontinuity B5) locally presents paleokarst features with
675 reddish clay infills, suggesting subaerial exposure (Fig. 11H). The discontinuity also represents
676 an abrupt facies change from the shallow marine deposits of the uppermost Oliete Fm to the
677 continental coal-bearing clays and sandstones of the Escucha Fm (Fig. 11I).

678 **6 Discussion: palaeogeographic remarks and distribution of benthic fauna**

679 The palaeogeography of the Oliete Subbasin changed significantly around the Barremian-Aptian
680 transition. During most of the Barremian, it developed as a mostly isolated basin, which
681 experienced only occasional marine influence via a small ephemeral connection to the Morella
682 Subbasin (Aurell et al., 2018). During deposition of the uppermost Barremian-lowermost Aptian
683 Alacón Fm, a prolonged stage of sea-level rise at least partially driven by tectonics led to the
684 stepwise opening of a wide, shallow, and high-energy seaway connecting the Oliete and Morella
685 subbasins (García-Penas et al., 2022). Following an episode of rapid sea-level fall during the
686 earliest Aptian, the Oliete Subbasin and its transition zones to the adjacent Las Parras and
687 Morella subbasins were subaerially exposed, generating a subbasin-wide karstified discontinuity
688 surface topping the Alacón Fm.

689 Deposition of the Aptian Josa and Oliete formations took place in a protected bay, which
690 included a wide spectrum of subenvironments (from coastal to shallow marine), with siliciclastic-
691 dominated (sequence J) to mixed sedimentation (sequences O1-O3). As documented in the
692 facies analysis, each subenvironment is characterised by a particular association of benthic
693 fauna (Fig. 14). The abundance and diversity of groups such as bivalves, gastropods and

694 echinoderms observed in the Oliete Bay contrast with the absence or scarcity of other benthic
695 groups, such as rudists and colonial corals, which formed massive accumulations in adjacent
696 open platform areas of the same age in the Las Parras, Galve and Morella subbasins (Fig. 1B).
697 The factors controlling the observed distribution of the benthic fauna are discussed below.

698 **6.1 Influence of paleeogeography on environmental factors in the Oliete Subbasin**

699 In the Maestrazgo Basin, the Mesozoic sedimentary record is often incomplete or absent in the
700 zones linking the different sedimentary domains (i.e. subbasins), as major extensional bounding
701 faults were reactivated forming thrusts during Cenozoic compression, leading to the uplift and
702 erosion of these areas (e.g., Simón and Liesa, 2011; Martín-Chivelet et al., 2019). However,
703 understanding transitional areas between subbasins can be the key to understanding the array
704 of factors (water depth and energy, degree of marine circulation and restriction, riverine inputs)
705 controlling the distribution of the benthic fauna across different subbasins.

706 During the Aptian, the Oliete Subbasin was a very compartmentalized marginal domain (Fig. 8A)
707 characterized by relatively restricted environments. The existence of extensive shoal belts in the
708 low-subsidence transitional area between the Oliete and Morella subbasins has been proposed
709 as the main cause of geographical restriction during the Barremian-early Aptian (García-Penas
710 et al., 2022), although direct evidence of the existence of these shoals during the late Aptian is
711 scarce due to extensive erosion. At Andorra and Berge (An log and control point 10, Fig. 1C), a
712 thick cross-stratified interval overlies the transgressive hemicycle of sequence J, and is overlain
713 by the latest Aptian-early Albian Escucha Fm (Fig. 12C, 2M). This interval is composed of high-
714 energy intraclastic grainstones (Fig. 4L) and is interpreted to be to the lateral equivalent of the
715 regressive hemicycle of Sequence J and of at least part of the Oliete sequences. This implies the
716 existence of high-energy shallow-marine areas in the Andorra-Molinos area during the late
717 Aptian, coeval with low-energy lagoonal environments inside the Oliete subbasin. The existence
718 of this shallow barrier is supported by the occasional presence of resedimented intraclastic

facies in the uppermost part of sequence J in Ariño and Barranco del Moro (Fig. 1B, 3), occasionally forming lobe-shaped beds migrating to the SW, away from the elevated shoal areas and towards the deeper areas of the lagoon (Fig. 7C).

In Montalbán, at the southern boundary of the Oliete Subbasin, the regressive hemicycle of sequence J is dominated by very coarse siliciclastic sediments. The overlying sequences O1-O3 are composed of mud-supported units preserving large articulated oysters as well as cassiopid and small turriculate gastropods, which are abundant components of low-energy stressed nearshore environments (e.g. Radley and Barker, 1998, 2000; Radley and Allen, 2000). This lithology and faunal content contrasts again with the open-marine carbonate-dominated successions with abundant colonial corals and rudists found immediately southwards in the Las Parras and Morella subbasins (Canérot, 1974; Clariana, 1999; Vennin and Aurell, 2001; Bover-Arnal et al., 2010, 2012, 2016; Peropadre, 2008, 2011), suggesting the existence of a geographical barrier separating both subbasins. Due to extensive erosion of the areas affected by compression around the Utrillas Fault System (Simón and Liesa, 2011; see also Fig. 5), it is difficult to ascertain the exact nature of the connection between the Oliete and Las Parras subbasins during the Aptian. However, the development of very localized carbonate-dominated environments with abundant green algae in the southern areas of the Oliete Subbasin in the uppermost part of Sequence J (Estercuel, Figs. 6, 8B) supports the existence of at least episodic communication between both subbasins.

The complete absence of rudists in the Oliete Subbasin was probably influenced by the extensive shoal belts bounding the subbasin. These shoals would have severely hindered marine circulation, making it difficult for the planktonic larvae of rudists (Gili and Götz, 2018) to even reach the Oliete Subbasin. Inside the subbasin, frequent salinity variations with prolonged episodes of lowered salinity, high siliciclastic input, shifting substrates and bottom hypoxia would have inhibited the development of rudist assemblages.

744 The elevated environmental stress and geographical restriction of the Oliete Subbasin also
745 influenced the distribution of other groups, such as decapod crustaceans. The siliciclastic-
746 dominated Josa Fm is characterised by a predominance of generalist groups such as axiidean
747 shrimps and glypheid lobsters (Ferratges et al., 2021), which could tolerate the unstable
748 environmental conditions of the Oliete Bay. Decapod faunas in the overlying Oliete Fm have not
749 been studied in detail, but seem to be composed mainly of thalassinid shrimps s.l. (García-Penas
750 et al., 2022), which are typical inhabitants of proximal lagoonal environments with changing
751 salinity levels (e.g., Hyžný et al., 2015). García-Penas et al. (2023) discussed in depth the
752 distribution of Lower Cretaceous decapod crustacean faunas across the Maestrazgo Basin.

753 The local occurrence of scarce in-situ colonial corals in Sequence O1 at Ariño and Barranco del
754 Moro (Fig. 1C) is also relevant. These organisms require clear and well-oxygenated waters with
755 normal marine salinity in order to grow. Given the proximity of these localities to the transition
756 area between the Oliete and Morella subbasins (see also Section 7), it is interpreted that stable
757 marine conditions probably were maintained in the northeastern part of the Oliete Bay at this
758 stage through the Andorra-Molinos seaway, allowing the development of coral colonies.

759 **6.2 Oscillating biodiversity in an early Aptian delta-influenced system**

760 The different subenvironments recognised during the sedimentation of the Josa Fm (i.e., from
761 siliciclastic coastal plain to offshore-prodelta settings, see Fig. 14) includes particular benthic
762 associations, with the local dominance of different types of bivalves. Orbitolinids are also
763 dominant in local skeletal beds interbedded between the offshore clays.

764 The lower offshore clays of the Josa Fm are characterised by high-diversity decapod associations
765 (Ferratges et al., 2021) and normal marine benthic taxa, including solitary corals, echinoids,
766 pectinid bivalves and oysters. Distinct beds of orbitolinid floatstone intercalated between clayey
767 offshore facies contain well-preserved discoidal forms of autochthonous or parautochthonous
768 *Palorbitolina lenticularis*. *Palorbitolina* blooms were common during the late Barremian-early

769 Aptian of the Maestrazgo Basin (e.g., Canérot, 1972; Aurell et al., 2001; Bover-Arnal et al., 2010)
770 and other basins of the Western Tethys (see Huck et al., 2013 and references therein). Flattened
771 discoidal forms of orbitolinids are commonly interpreted to have inhabited deeper-water
772 environments than conical counterparts (e.g., Rahiminejad and Hassani, 2016). However, in the
773 Maestrazgo Basin, blooms of discoidal orbitolinids have been recorded in very shallow facies
774 with increased detrital quartz content (Peropadre, 2011). The uniformly flat *Palorbitolina*
775 morphotypes found in the offshore clays of the Josa Fm are remarkably different from the
776 subconical forms found in the shallower-water deposits of the underlying Alacón Fm (García-
777 Penas et al., 2022), suggesting that the morphological variability of *Palorbitolina* in the Oliete
778 Subbasin was indeed controlled by bathymetry. Orbitolinid floatstones occur around the turning
779 point between offshore marls and delta-influenced siliciclastic prodelta clays and sandstones,
780 suggesting that blooms of orbitolinids developed under specific environmental conditions, with
781 increased riverine nutrient inputs, but still under a relatively stable marine regime, as indicated
782 by the co-occurrence of orbitolinids and solitary corals (Fig. 2C).

783 The uppermost part of the Josa Fm at the western margin of the Oliete Subbasin (Josa, Obón)
784 corresponds to siliciclastic littoral facies preserving high-diversity bivalve associations (e.g.
785 Coquand, 1865; Mallada, 1878), dominated by trigoniids and oysters. Trigoniids are shallow
786 burrowing bivalves that commonly inhabited well-oxygenated shoreface environments with
787 normal marine salinity, in depths of around 10-15 m (Komatsu, 1999; Francis and Hallam, 2003;
788 Lazo, 2004, 2007), although some groups, such as pterotrigoniids, were able to adapt to tidal
789 flat environments (Komatsu and Maeda, 2005).

790 The abundance and diversity in the siliciclastic littoral facies of autochthonous and
791 parautochtonous euhaline taxa such as trigoniids and other large bivalves (Table 2) contrasts
792 with the near absence of foraminifera, green algae, and other euhaline markers such as
793 bryozoans and cephalopods. Bioturbation in these littoral facies is scarce and consists only of

794 *Ophiomorpha* isp. and *Thalassinoides* isp., which are common in brackish shoreface
795 environments (Hubbard et al., 2004; Buatois et al., 2005; Pemberton et al., 2012). Also abundant
796 are ostracods, which thrive under a variety of environmental conditions, and abraded
797 orbitolinids, which could easily have been transported by storms from offshore environments.
798 Based on these features, we regard the faunal composition in the upper part of the Josa Fm as
799 the result of time-averaging of different faunal associations adapted to variable environmental
800 conditions in a shallow delta front. Episodes of increased runoff would have promoted the
801 development of euryhaline communities dominated by oysters and cassiopid gastropods
802 (Cleevely and Morris, 1988; Banjac et al., 2007). Periodically, episodes of reduced freshwater
803 input would have allowed the proliferation of more diverse mollusc assemblages dominated by
804 trigoniids, which would have thrived in the shallow waters with increased nutrient
805 concentrations of the delta front. The abundance of trigoniids in the Josa-Obón area was very
806 probably controlled not only by variations of salinity and nutrient availability, but also by the
807 occurrence in these proximal areas of fine quartz sand substrates, to which this group of bivalves
808 was particularly well adapted (Stanley, 1970).

809 **6.3 Faunal zonation in a late Aptian protected lagoon**

810 The palaeogeographic configuration of the Oliete Subbasin is interpreted to have remained
811 broadly unchanged during deposition of the late Aptian Oliete sequences O1-O3. During these
812 intervals, the Oliete Bay resembled a large protected lagoon, sheltered from direct marine
813 influence by large non-migrating barriers (Fig. 8 C-D-E). The low diversity microfaunal
814 associations (i.e. scarce green algae, ostracods, agglutinated foraminifera) found throughout
815 sequences O1 and O2 suggest a certain degree of environmental stress, attributed mainly to
816 salinity oscillations and unstable substrates, and possibly to episodic hypoxia.. The
817 environmental restriction of the Oliete lagoon is also reflected in the composition of the
818 macrofaunal associations (Fig. 14).

In Sequence O1, deeper environments characterize the depocentral area of the subbasins (Alacón, Cabezo Negro; Figs. 7B, 9). There, it is dominated by thick unfossiliferous clay intervals with rare tempestitic interbeds. The lack of fauna could be explained by persistent bottom hypoxia caused by a meromictic regime due to reduced water circulation. Bottom-water stagnation is common in low-energy coastal basins with restricted connection to open seas (e.g., Gravina et al., 1989; Xia and Jiang, 2015; Rigaud et al., 2021), especially if the barrier separating them from open seas is significantly shallower than the basin itself, impeding the effective mixing of the deeper water layers (Witzke, 1987; Rakshit et al., 2023).

The deepest areas of the protected lagoon were flanked by low-energy mud-dominated environments colonised by a variety of infauna and epifauna. The mollusc associations are dominated by bivalves, mostly by members of Arcidae and Veneridae, which are capable of tolerating salinity fluctuations into the brachyhaline range by closing off their valves and retreating into their burrows (e.g., Davenport and Wong, 1986; Abele and Philipp, 2013; Mendoza et al., 2017; Pourmozaffar et al., 2020; Woodin et al., 2020). The gastropod association, with large cassiopid, turritellid and cerithiids is typical of very proximal marine environments (Allmon, 1988; Cleevely and Morris, 1988; Radley and Barker, 1998; Flügel, 2010). This benthic faunal association also contains abundant euryhaline *Crassostrea*, which thrivd in mesohaline to brachyhaline salinities (Moore, 1971; Kondo et al., 2006), and various morphotypes of Gryphaeidae, which adopted a reclining mode of life on soft substrates in low-energy environments (Kosenko, 2014). Although gryphaeid oysters have classically been considered an euhaline group (Stenzel, 1971), several studies have linked the mass occurrence of Gryphaeidae to lowered or oscillating salinities (Calzada-Badía and Botero-Arango, 1979; Ten Hove and Van den Hurk, 1993; Gámez et al., 2003; Ferrer and Gibert, 2005; Lazo et al., 2008; García-Penas et al., 2022).

The westerly coastal plain areas of the Blesa inlet were occupied by oyster banks (*Crassostrea* and gryphaeids) and serpulids, a faunal association commonly found in shallow environments with fluctuating salinities (Andrews and Walton, 1990; Flügel, 2010). *Crassostrea* is a gregarious oyster that specialized in colonizing intertidal to shallow subtidal muddy environments, where individuals adopt a vertical position forming bouquet-like colonies in the muddy substrate. This behaviour helps the oysters to avoid burial in soupy substrates, thanks to their characteristic elongated shape and a shell microstructure formed by thin interlocking calcite laminae and large empty spaces, which greatly decreases shell density and increases buoyancy (Stenzel, 1971; Komatsu et al., 2002).

The coastal oyster and serpulid banks probably acted as effective baffles (Chauvin, 2018; Morris et al., 2019) against the weak fair-weather wave-action and tidal currents of the Oliete subbasin, allowing the development of the extensive low-energy "backbarrier" mudflats observed in Blesa, Estercuel and Montalbán, inhabited by large oysters and other opportunistic bivalves and gastropods.

Sequence O3 is characterised by the basinwide occurrence of glauconitic and peloidal facies, locally characterised by unusually high concentrations of *Thalassinoides* bioturbation (Fig. 3I) and localised ripple cross-lamination, evidencing a shallow-marine low-energy environment similar to the upper part of the underlying Sequence O2. However, while Sequence O2 is characterised by restricted microfaunal associations, Sequence O3 contains diverse associations of benthic foraminifera, including the basinwide reappearance of orbitolinids, often in association with calcareous green algae (Fig. 4I). These faunal associations are characteristic of well-oxygenated shallow-water environments with low to moderate energy levels, situated in the photic zone and with normal-marine salinity (Flügel, 2010; Wray, 1977), a set of conditions typical of open coastal lagoons (e.g., Pittet et al., 2002; Rahiminejad and Hassani; 2016). This implies an attenuation of any ecological stressors present in sequences O1 and O2 during

deposition of Sequence O3 (i.e., salinity variations, episodic bottom hypoxia), which had been favoured by a restricted connection between the Oliete Subbasin and the open-marine seas of the Morella and Las Parras subbasins.

The upper part of Sequence O3 is also characterised by the appearance of beds of cross-stratified bioclastic-peloidal grainstone, interpreted as subtidal dunes migrating towards the deeper parts of the bay, probably generated by storm return currents (Fig. 8E). All observed features suggest an increase in environmental energy and marine circulation relative to O2. We rule out sea-level rise as the driver of this increase in connection with open seas, as sequence O3 is dominated by very proximal shallow environments, which may suggest a stabilization or decrease in water depth compared to Sequence O2. Sinsedimentary tectonics significantly conditioned deposition in the southeastern margin of the Oliete Subbasin during the Barremian and Aptian (Rodríguez-López et al., 2007; García-Penas et al., 2022). In the Andorra-Molinos area, the Aptian succession unconformably overlies a folded and tilted Jurassic substrate (Fig. 12C), evidencing synsedimentary tectonic activity during the Early Cretaceous. Accordingly, we interpret that localised fault activity in the Andorra-Molinos linkage area during the late Aptian could have opened a deeper and stable connection with the Morella subbasin during deposition of sequence O3, allowing for more effective marine circulation between both subbasins (Fig. 8E).

6.4 Past and present analogues of the Josa and Oliete formations:

The transgressive flooding of low-relief coastal areas can give rise to a wide variety of coastal shallow-marine features, such as bays, estuaries and lagoons (Kjerfve, 1994; Duck and da Silva, 2012). The existence of these features depends directly on the local relative rate of sea-level change, which frequently makes them short-lived on a geologic time frame and prone to rapid environmental variations (Kjerfve, 1994).

The early Aptian Josa Formation defined in this study was sedimented in a marginal bay during a long-term transgressive-regressive cycle, with stressed environmental conditions derived from

fluvial influence. The transgressive and early regressive intervals are composed of clays with orbitolinids, decapod crustaceans and otherwise low-diversity faunal assemblages of small solitary corals and bivalves. The late regressive stage is dominated by delta front sandstones and storm-influenced subtidal mixed dunes. Faunal associations in these regressive materials are dominated by bivalves and gastropods, mostly trigoniids, oysters, venerids, arcids, cassiopids and turritellids.

The Aptian Romualdo Formation, in the Araripe Basin of northwestern Brazil, represents an analogous environment to the Josa Fm, although with a higher degree of restriction (e.g. Fürsich et al., 2019; Kroth et al., 2021). The Romualdo Formation overlies continental playa-lake evaporites (do Nascimento et al., 2016), and comprises a single depositional sequence (Custódio et al., 2017). The transgressive systems tract (TST) of the sequence is composed of alluvial and tide-influenced clays and sandstones, overlain by shallow-marine dark shales with carbonate fossiliferous concretions containing crustaceans, plants and vertebrate remains. The early highstand systems tract (HST) is composed of dark shales with interbedded wave-influenced coquinas dominated by bivalves and gastropods (Kroth et al., 2021). The late HST comprises tidally influenced cross-bedded sandstones. The low-diversity faunal associations of the coquinas are dominated by venerid, lucinid and mytilid bivalves, and various cassiopid gastropods (Fürsich et al., 2019). Decapod crustaceans are also abundant in the shales of the lower HST, and occur both as flattened remains and in carbonate concretions (Fürsich et al., 2019).

The Romualdo Formation is interpreted to represent deposition in a protected embayment comprising various discrete subenvironments (Kroth et al., 2021). Low-diversity faunal associations in the TST evidence high environmental stress, attributed to dysoxic conditions and salinity oscillations (Fürsich et al., 2019). The siliciclastic late HST deposits shows the progradation of small deltaic systems (Fürsich et al., 2019; Kroth et al, 2021). The embayment

may have been connected to the Central North Atlantic Ocean via a narrow seaway (Assine et al., 2016; Kroth et al., 2021).

The late Aptian Oliete Formation has been interpreted in this study as a particular example of a lagoonal system developed in a tectonically-controlled marginal basin. This system contained an array of low-energy shallow-marine environments characterised by specific benthic communities. The marginal areas of the Oliete lagoon are characterised by intertidal to shallow subtidal environments subject to fluvial influence, which were inhabited by mass oyster accumulations locally associated with mass-occurrences of venerid bivalves and turritellid gastropods. The deeper mud-dominated areas of the lagoon were inhabited by relatively diverse associations of bivalves and gastropods.

Lagoonal environments bearing a close resemblance to the late Aptian Oliete Formation have been described in the Myakka Lagoon System (MLS) (Petuch, 2004), a complex and dynamic system of estuaries, lagoons and emerged islands which developed in the low-lying areas of western Florida during the Pliocene and Pleistocene. The evolution of these tropical coastal environments was conditioned by rapid eustatic sea-level changes tied to climatic oscillations (Petuch, 2004; Hine et al., 2017).

The open areas of the Myakka Lagoon System facing the ocean were dominated by diverse communities of epifaunal and infaunal bivalves, including pectinids, arcids, cardiids, semelids and tellinids, and a wide variety of gastropods. The shallow mud-dominated inner lagoons were inhabited by communities of shallow infaunal bivalves dominated by venerids and a variety of gastropods (Petuch, 2004).

Mass-accumulations of turritellid gastropods controlled by nutrient inputs occurred in the proximal areas of the lagoons. Single-species accumulations of grypheid oysters associated with encrusting polychaete worms and gastropods proliferated in the very shallow and sheltered coastal areas. Extensive intertidal mud flats developed in the low-relief areas close to the

943 exposed reliefs of the Florida Peninsula. These intertidal to very shallow subtidal environments
944 were occupied by mangrove jungles which hosted mass accumulations of *Crassostrea* (Petuch,
945 2004).

946 Another analogue for the environmental conditions of the Oliete Lagoon can be found in the
947 Ten Thousand Islands of present-day western Florida. The Ten Thousand Islands are a complex
948 system of small islands, bays and lagoons developed during the Holocene transgression of the
949 Pacific Ocean over the Florida coastline (Petuch and Berschauer, 2022). The system is composed
950 of two groups of islands with markedly different sets of environmental conditions. The Outer
951 Ten Thousand islands, which group the seaward islands and lagoons, are characterised by
952 extensive vermetid gastropod reefs, sandy sediment and relatively stable marine conditions. The
953 Inner Ten Thousand Islands (ITTI) represent a group of protected bays, lagoons and islands
954 adjacent to the mainland, which are characterised by intense riverine influence, restricted
955 marine circulation and changing water salinity levels which oscillate between oligohaline and
956 slightly hypersaline (Soderqvist and Patino, 2010). The innermost coastline of the ITTI is
957 composed by small protected embayments with highy unstable salinities. The muddy bottoms
958 of the embayments are colonised almost exclusively by banks of the oysters *Crassostrea* and
959 *Ostreola* (Petuch and Berschauer, 2022). Seaward of the oyster-dominated bays, in the
960 nearshore lagoons of the ITTI, salinity oscillations are less extreme, and the muddy bottoms
961 support large seagrass meadows, which host diverse communities of small bivalves and
962 gastropods. Bivalve associations are impoverished compared to open marine areas, and include
963 arcids, mytilids, pectinids, pinnids, lucinids, carditids, venerids, tellinids, pholadids, tellinids and
964 corbulids (Petuch and Myers, 2014).

965 **7. Conclusions**

966 1. This work describes the Aptian sedimentary evolution and palaeogeography of a
967 shallow-marine protected bay at the eastern margin of Iberia (Oliete Subbasin,

968 Maestrazgo Basin), connected to the open sea by a low-subsidence non-moving shoal
969 area.
970 2. Four transgressive-regressive (T-R) third-order sequences have been identified,
971 bounded by five basinwide-correlatable discontinuities interpreted as maximum
972 regressive surfaces. Discontinuities B1 and B2 constrain sequence J, which includes a
973 siliciclastic-dominated succession (Josa Fm) representing a variety of proximal, deltaic-
974 influenced environments. Faunal associations include diverse bivalve faunas dominated
975 by oysters and trigoniids. Discontinuities B1 and B2 present clear evidence of subaerial
976 exposure during the early Aptian.
977 3. Sequences O1 and O2 encompass the lower and middle Oliete Fm, and include
978 carbonate-dominated lagoonal facies. Diverse in-situ accumulations of articulated
979 bivalves, cassiopid gastropods and green algae characterise the deeper parts of the
980 lagoon. The marginal areas are characterised by mud-dominated accumulations of
981 articulated oysters and serpulids, and by the local development of siliciclastic coastal
982 plains. A single bed of bioclastic grainstone with abundant iron ooids is associated with
983 the upper boundary of Sequence O1; ooids probably originated in marginal lateritic
984 paleosols which were reworked during early sea-level rise.
985 4. Sequence O3 records a generalised increase in environmental energy and marine
986 circulation in the Oliete Bay lagoon, evidenced by increased microfaunal diversities and
987 the occurrence of high-energy peloidal-bioclastic dune deposits across the lagoon,
988 which probably indicates increased connection between the Oliete Bay and the open
989 seas of the Maestrazgo Basin in a regressive context. This increased connection was
990 possibly driven by tectonic activity at the southeastern margin of the Oliete Subbasin.
991 5. Mass-accumulations of glauconite are associated with the transgressive stage of
992 Sequence O3. These accumulations occur in very shallow subtidal to intertidal

conditions, and could be related to the transgressive reworking of intertidal siliciclastics underlying Sequence O3.

Acknowledgements

This study was financially supported by the Spanish Ministerio de Economía y Competitividad (project CGL2017-85038-P), and by the Aragón Regional Government and European Regional Development Fund (research group E18_20R Aragosaurus: recursos geológicos y palaeoambientes). Álvaro García-Penas has a predoctoral contract (contract code PRE2018-084468), co-financed by the Spanish Government and the European Social Fund (ESF). We appreciate the technical assistance of the Servicio General de Apoyo a la Investigación-SAI, Universidad de Zaragoza. We are deeply grateful to three anonymous reviewers for their insightful revision of the original manuscript, as well as to Dr. Franz Fürsich and an anonymous reviewer for their detailed evaluation of the second iteration of the manuscript. We feel that their comments and suggestions have greatly improved the presentation and general quality of this work. We would also like to thank the Editor in Chief, Dr. Massimo Moretti, for his assistance during the review process..

References

Abdelhady, A.A., Seuss, B., Fürsich, F.T., Ali, A., Abdel-Raheem, K.H.M., Mohamed, R.S.A., 2020. Paleoenvironmental significance of the monospecific biostromes in the Campanian-Maastrichtian Duwi Formation (Eastern Desert, Egypt). Sedimentary Geology 408, 105772. https://doi.org/10.1016/j.sedgeo.2020.105772

Abele, D., Philipp, E., 2013. Environmental control and control of the environment: The basis of longevity in bivalves. Gerontology 59, 261–266. https://doi.org/10.1159/000345331

1016 Aguirre-Urreta, M.B., Lazo, D.G., Griffin, M., Vennari, V.V., Parras, A.M., Cataldo, C.,
1017 Garberoglio, R., 2011. Megainvertebrados del cretácico y su importancia bioestratigráfica.
1018 Relatorio del XVIII Congreso de Geológico Argentino, Neuquén 465–488.

1019 Aigner, Thomas., 1985. Storm depositional systems : dynamic stratigraphy in
1020 modern and ancient shallow-marine sequences. Springer-Verlag.

1021 Allmon, W.D., 1988. Ecology of recent turritelline gastropods (Prosobranchia,
1022 Turritellidae): current knowledge and paleontological implications. Palaios 3, 259–284.
1023 https://doi.org/10.2307/3514657

1024 Allmon, W.D., 2011. Natural history of turritelline gastropods (Cerithiodea:
1025 Turritellidae): A status report. Malacologia 54, 159–202.
1026 https://doi.org/10.4002/040.054.0107

1027 Andrews, J.E., Walton, W., 1990. Depositional environments within Middle Jurassic
1028 oyster-dominated lagoons: an integrated litho-, bio- and palynofacies study of the Duntulm
1029 Formation (Great Estuarine Group, Inner Hebrides). Transactions of the Royal Society of
1030 Edinburgh: Earth Sciences 81, 1–22.

1031 Anthony, E.J., 2015. Wave influence in the construction, shaping and destruction of
1032 river deltas: A review. Marine Geology 361, 53–78.
1033 https://doi.org/10.1016/j.margeo.2014.12.004

1034 Ashton, A.D., Giosan, L., 2011. Wave-angle control of delta evolution. Geophysical
1035 Research Letters 38. https://doi.org/10.1029/2011GL047630

1036 Assine, M.L., Quaglio, F., Warren, L.V., Simões, M.G., 2016. Comments on paper by
1037 M. Arai “Aptian/Albian (Early Cretaceous) paleogeography of the South Atlantic: a
1038 paleontological perspective.” Brazilian Journal of Geology 46, 03–07.
1039 https://doi.org/10.1590/2317-4889201620150046A

Aurell, M., Fregenal-Martínez, M., Bádenas, B., Muñoz-García, M.B., Élez, J., Meléndez, N., de Santisteban, C., 2019. Middle Jurassic–Early Cretaceous tectono-sedimentary evolution of the southwestern Iberian Basin (central Spain): Major palaeogeographical changes in the geotectonic framework of the Western Tethys. Earth-Science Reviews 199, 102983. https://doi.org/10.1016/j.earscirev.2019.102983

Aurell, M., Soria, A.R., Bádenas, B., Liesa, C.L., Canudo, J.I., Gasca, J.M., Moreno-Azanza, M., Medrano-Aguado, E., Meléndez, A., 2018. Barremian synrift sedimentation in the Oliete sub-basin (Iberian Basin, Spain): palaeogeographical evolution and distribution of vertebrate remains. Journal of Iberian Geology 44, 285–308. https://doi.org/10.1007/s41513-018-0057-3

Bádenas, B., Aurell, M., 2001. Proximal-distal facies relationships and sedimentary processes in a storm dominated carbonate ramp (Kimmeridgian, Northwest of the Iberian Ranges, Spain. Sedimentary Geology 139, 319–340. https://doi.org/10.1016/S0037-0738(00)00151-2

Bádenas, B., Aurell, M., Gasca, J.M., 2018. Facies model of a mixed clastic–carbonate, wave-dominated open-coast tidal flat (Tithonian–Berriasian, north-east Spain). Sedimentology 65, 1631–1666. https://doi.org/10.1111/sed.12441

Banerjee, S., Bansal, U., Vilas Thorat, A., 2016. A review on palaeogeographic implications and temporal variation in glaucony composition. Journal of Palaeogeography 5, 43–71. https://doi.org/10.1016/j.jop.2015.12.001

Banjac, N., Bandel, K., Kiel, S., 2007. Cassiopid gastropods from the Cretaceous of Western Serbia. Geoloski anali Balkanskoga Poluostrva 68 (1), 61–71. https://doi.org/10.2298/gabp0701061b

Bansal, U., Banerjee, S., Pande, K., Ruidas, D.K., 2020. Unusual seawater composition of the Late Cretaceous Tethys imprinted in glauconite of Narmada Basin, central India. Geological Magazine 157, 233–247. https://doi.org/10.1017/S0016756819000621

Bansal, U., Böning, P., Wilmsen, M., 2023. Enhanced chemical weathering of the continents promoted fast Late Cretaceous nearshore glaucony formation: implications from the Danubian Cretaceous Group, Germany. Journal of the Geological Society 180, 1–15. https://doi.org/10.6084/m9.figshare.c.6297404

Bataller, J.R., 1947. Sinopsis de las especies nuevas del Cretácico de España. Anales de la Escuela de Peritos Agrícolas y de Especialidades Agropecuarias y de los Servicios Técnicos de Agricultura 6, 2–186.

Bhattacharya, J.P., 2010. Deltas, in: Facies Models. Geological Association of Canada, pp. 233–265.

Bhattacharya, J.P., Giosan, L., 2003. Wave-influenced deltas: Geomorphological implications for facies reconstruction. Sedimentology 50, 187–210. https://doi.org/10.1046/j.1365-3091.2003.00545.x

Bhattacharya, J.P., Walker, R.G., 1992. Deltas, in: Facies Models: Response to Sea Level Change. Geological Association of Canada, St Johns, pp. 157–177.

Bover-Arnal, T., Löser, H., Moreno-Bedmar, J.A., Salas, R., Strasser, A., 2012. Corals on the slope (Aptian, Maestrat Basin, Spain). Cretaceous Research 37, 43–64. https://doi.org/10.1016/j.cretres.2012.03.001

Bover-Arnal, T., Moreno-Bedmar, J.A., Frijia, G., Pascual-Cebrian, E., Salas, R., 2016. Chronostratigraphy of the Barremian – Early Albian of the Maestrat Basin (E Iberian

Peninsula): integrating strontium-isotope stratigraphy and ammonoid biostratigraphy. Newsletters on Stratigraphy 49, 41–68. https://doi.org/10.1127/nos/2016/0072

Bover-Arnal, T., Moreno-Bedmar, J.A., Salas, R., Skelton, P.W., Bitzer, K., Gili, E., 2010. Sedimentary evolution of an Aptian syn-rift carbonate system (Maestrat Basin, E Spain): Effects of accommodation and environmental change. Geologica Acta 8, 249–280. https://doi.org/10.1344/105.000001533

Bover-Arnal, T., Salas, R., Guimerà, J., Moreno-Bedmar, J.A., 2022. Eustasy in the Aptian world: A vision from the eastern margin of the Iberian Plate. Global and Planetary Change 214, 103849. https://doi.org/10.1016/j.gloplacha.2022.103849

Buatois, L.A., Gingras, M.K., MacEachern, J., Mángano, M.G., Zonneveld, J.P., Pemberton, S.G., Netto, R.G., Martin, A., 2005. Colonization of brackish-water systems through time: Evidence from the trace-fossil record. Palaios 20, 321–347. https://doi.org/10.2110/palo.2004.p04-32

Caja, M.A., 2004. Procedencia y diagénesis de los sedimentos del Jurásico superior Cretácico Inferior (Facies Weald) en las subcuencas Occidentales de la Cuenca del Maestrazgo, Cordillera Ibérica oriental. Universidad Complutense de Madrid.

Calzada, S., Botero, G., 1979. *Ceratostreon tuberculiferum landereri*, n. ssp. del Aptiense español (Ostreidae). Estudios Geologicos 35, 459–464.

Canérot, J., 1974. Recherches géologiques aux confins des chaines ibérique et catalane (Espagne). PhD Thesis, Université Paul Sabatier.

Canérot, J., Cugny, P., Murat, B., 1982a. Le bassin eocrétacé d'Oliete (province de Teruel, Espagne): un modèle de bassin de plate-forme instable. Cuadernos de Geología Ibérica 8, 267–282.

Canérot, J., Cugny, P., Pardo, G., Salas, R., Villena, J., 1982b. Ibérica Central-Maestrazgo, in: García, A. (Ed.), El Cretácico de España. Universidad Complutense de Madrid, Madrid, pp. 273–344.

Casas Sáinz, A., Cortés Gracia, A., Liesa Carrera, C., Meléndez Hevia, A., Soria de Miguel, A., 1997. Estructura del borde N de la Cordillera Ibérica entre la Sierra de Arcos y el anticlinal de Montalbán. Cuadernos de Geología Ibérica 23, 243–268. https://doi.org/10.5209/rev_CGIB.1997.v23.2494

Cattaneo, A., Steel, R.J., 2003. Transgressive deposits: a review of their variability. Earth-Science Reviews 62, 187–228. https://doi.org/10.1016/S0012-8252(02)00134-4

Catuneanu, O., Abreu, V., Bhattacharya, J.P., Blum, M.D., Dalrymple, R.W., Eriksson, P.G., Fielding, C.R., Fisher, W.L., Galloway, W.E., Gibling, M.R., Giles, K.A., Holbrook, J.M., Jordan, R., Kendall, C.G.S.C., Macurda, B., Martinsen, O.J., Miall, A.D., Neal, J.E., Nummedal, D., Pomar, L., Posamentier, H.W., Pratt, B.R., Sarg, J.F., Shanley, K.W., Steel, R.J., Strasser, A., Tucker, M.E., Winker, C., 2009. Towards the standardization of sequence stratigraphy. Earth-Science Reviews 92, 1–33. https://doi.org/10.1016/j.earscirev.2008.10.003

Chakrabarty, S., Shukla, M., Gorai, D., 2022. Origin and significance of glauconites in a sequence stratigraphic perspective: Sylhet Formation, Assam and Assam–Arakan Basin, India. Journal of Earth System Science 131 (3), 1-24, . https://doi.org/10.1007/s12040-022-01887-0

Chauvin, J., 2018. Wave Attenuation by Constructed Oyster Reef Breakwaters . MsC Thesis, Louisiana State University and Agricultural and Mechanical College. https://doi.org/10.31390/gradschool_theses.4752

1131 Clariana, M.P., 1999. Estratigrafía y sedimentología de las facies Urgon (Aptiense)
1132 en la subcuenca de Las Parras (Provincia de Teruel) (Tesis de Licenciatura). Universidad de
1133 Zaragoza.

1134 Clariana, M.P., Meléndez, A., 2000. Los depósitos terrigenos de la base de la
1135 secuencia de depósito Aptiense superior. Subcuenca de las Las Parras (provincia de Teruel).
1136 Geogaceta 27, 43–45.

1137 Clariana, M.P., Meléndez, A., Soria, A.R., 2000. Sedimentología y paleogeografía de
1138 la secuencia de depósito Aptiense inferior (facies Urgon) en la subcuenca de Las Parras
1139 (Teruel). Geogaceta 27, 47–50.

1140 Cleevely, R.J., Morris, N.J., 1988. Taxonomy and ecology of Cretaceous Cassiopidae
1141 (Mesogastropoda). Bulletin of the British Museum (Natural History), Geology Series 44,
1142 233–291.

1143 Coquand, H., 1865. Monographie de l'Étage Aptien de L'Espagne. Imprimeurs de la
1144 Société d'Émulation, Marseille.

1145 Cuitiño, J.I., Santos, R.V., Scasso, R.A., 2013. Insights into the distribution of shallow-
1146 marine to estuarine early miocene oysters from southwestern patagonia: Sedimentologic
1147 and stable isotope constraints. Palaios 28, 583–598.
1148 https://doi.org/10.2110/palo.2012.p12-105r

1149 Custódio, M.A., Quaglio, F., Warren, L.V., Simões, M.G., Fürsich, F.T., Perinotto,
1150 J.A.J., Assine, M.L., 2017. The transgressive-regressive cycle of the Romualdo Formation
1151 (Araripe Basin): Sedimentary archive of the Early Cretaceous marine ingression in the
1152 interior of Northeast Brazil. Sedimentary Geology 359, 1–15.
1153 https://doi.org/10.1016/j.sedgeo.2017.07.010Dalrymple, R.W., 1992. Tidal Depositional

1154 Systems, in: Facies Models: Response to Sea Level Change. Geological Association of Canada,
1155 St Johns, pp. 195–218.

1156 Dalrymple, R.W., Rhodes, R.N., 1995. Estuarine dunes and bars. Developments in
1157 Sedimentology 53, 359–422. https://doi.org/10.1016/S0070-4571(05)80033-0

1158 Dalvand, M., Ashrafzadeh, A.R., Ahmadi, Z., 2015. Crustacean microcoprolites from
1159 Lower Cretaceous and Oligo-Miocene deposits, Persian Gulf, Iran. Journal of
1160 Micropalaeontology 34, 211–216. https://doi.org/10.1144/jmpaleo2014-028

1161 Davenport, J., Wong, T.M., 1986. Responses of the blood cockle *Anadara granosa*
1162 (L.) (Bivalvia: Arcidae) to salinity, hypoxia and aerial exposure. Aquaculture 56, 151–162.
1163 https://doi.org/10.1016/0044-8486(86)90024-4

1164 do Nascimento, D.R., da Silva Filho, W.F., Freire, J.G., dos Santos, F.H., 2016.
1165 Syngenetic and diagenetic features of evaporite-lutite successions of the Ipubi Formation,
1166 Araripe Basin, Santana do Cariri, NE Brazil. Journal of South American Earth Sciences 72,
1167 315–327. https://doi.org/10.1016/j.jsames.2016.10.001

1168 Duck, R.W., Da Silva, J.F., 2012. Coastal lagoons and their evolution: A
1169 hydromorphological perspective. Estuarine, Coastal and Shelf Science 110, 2–14.
1170 https://doi.org/10.1016/j.ecss.2012.03.007

1171 Dumitrescu, M., Brassell, S.C., Schouten, S., Hopmans, E.C., Damsté, J.S.S., 2006.
1172 Instability in tropical Pacific sea-surface temperatures during the early Aptian. Geology 34,
1173 833–836. https://doi.org/10.1130/G22882.1

1174 El Albani, A., Meunier, A., Fürsich, F., 2005. Unusual occurrence of glauconite in a
1175 shallow lagoonal environment (Lower Cretaceous, northern Aquitaine Basin, SW France).
1176 Terra Nova 17, 537–544. https://doi.org/10.1111/j.1365-3121.2005.00646.x

Ferratges, F.A., Hyžný, M., Zamora, S., 2021. Taphonomy and systematics of decapod crustaceans from the Aptian (Lower Cretaceous) in the Oliete Sub-basin (Teruel , Spain). Cretaceous Research 122, 104767. https://doi.org/10.1016/j.cretres.2021.104767

Ferrer, O., de Gibert, J.M., 2005. Presencia de *Teredolites* en la Formación Arcillas de Morella (Cretácico Inferior, Castellón). Spanish Journal of Palaeontology 20, 39–47.

Flügel, E., 2010. Microfacies of Carbonate Rocks, Analysis, Interpretation and Application. Springer-Verlag, Berlin.

Föllmi, K.B., 2012. Early Cretaceous life, climate and anoxia. Cretaceous Research 35, 230–257. https://doi.org/10.1016/j.cretres.2011.12.005

Francis, A.O., Hallam, A., 2003. Ecology and evolution of Jurassic trigoniid bivalves in Europe. Lethaia 36, 287–304. https://doi.org/10.1080/00241160310005115

Fürsich, F.T., Custódio, M.A., Matos, S.A., Hethke, M., Quaglio, F., Warren, L.V., Assine, M.L., Simões, M.G., 2019. Analysis of a Cretaceous (late Aptian) high-stress ecosystem: The Romualdo Formation of the Araripe Basin, northeastern Brazil. Cretaceous Research 95, 268–296. https://doi.org/10.1016/j.cretres.2018.11.021

Fürsich, F.T., Freytag, S., Röhl, J., Schmid, A., 1995. Palaeoecology of benthic associations in salinity-controlled marginal marine environments: Examples from the Lower Bathonian (Jurassic) of the Causses (southern France). Palaeogeography, Palaeoclimatology, Palaeoecology 113, 135–172.

Fürsich, F.T., Kirkland, J.I., 1986. Biostratinomy and Paleoecology of a Cretaceous Brackish Lagoon. PALAIOS 1, 543–560. https://doi.org/10.2307/3514706

Fürsich, F.T., Oschmann, W., 1993. Shell beds as tools in basin analysis: the Jurassic of Kachchh, western India. Journal of the Geological Society 150, 169–185.

Gámez, D., Paciotti, P., Colombo, F., Salas, R., Gámez, D., Colombo, F., Salas, R., 2003. La Formación Arcillas de Morella (Aptiense inferior), Cadena Ibérica oriental (España): caracterización sedimentológica. Geogaceta 34, 191–194.

García, R., Moreno-Bedmar, J.A., Bover-Arnal, T., Company, M., Salas, R., Latil, J.L., Martín-Martín, J.D., Gomez-Rivas, E., Bulot, L.G., Delanoy, G., Martínez, R., Grauges, A., 2014. Lower Cretaceous (Hauterivian-Albian) ammonite biostratigraphy in the Maestrat Basin (E Spain). Journal of Iberian Geology 40, 99–112. https://doi.org/10.5209/rev_JIGE.2014.v40.n1.44090

García-Penas, A., Aurell, M., Zamora, S., 2022. Progressive opening of a shallow-marine bay (Oliete Subbasin, Spain) and the record of possible eustatic fall events near the Barremian-Aptian boundary. Palaeogeography, Palaeoclimatology, Palaeoecology 594, 110938. https://doi.org/10.1016/j.palaeo.2022.110938

García-Penas, Á., Ferratges, F.A., Moreno-Bedmar, J.A., Bover-Arnal, T., Gasca, J.M., Aurell, M., Zamora, S., 2023. Decapod crustaceans from the Lower Cretaceous of Spain, with an account of new occurrences in Barremian-Aptian strata of the Maestrazgo Basin. Cretaceous Research 105576. https://doi.org/10.1016/j.cretres.2023.105576

Geptner, A.R., Ivanovskaya, T.A., 2000. Glauconite from Lower Cretaceous Marine Terrigenous Rocks of England: A Concept of Biochemogenic Origin, Translated.from Litologiya i Poleznye Iskopaemye.

Gili, E., Götz, S., 2018. Treatise Online no. 103: Part N, Volume 2, Chapter 26B: Paleoecology of rudists. Paleontological Institute, University of Kansas, Lawrence.

Gladfelter, W.B., 1978. General Ecology of the Cassiduloid Urchin *Cassidulus caribbearum*. Marine Biology 47, 149–160.

Goldhammer, R.K., 1997. Compaction and Decompaction Algorithms for Sedimentary Carbonates. Journal of Sedimentary Research 67, 26–35.

Gravina, M.F., Ardizzone, G.D., Scaletta, F., Chimenz, C., 1989. Descriptive Analysis and Classification of Benthic Communities in Some Mediterranean Coastal Lagoons (Central Italy). Marine Ecology 10, 141–166. https://doi.org/10.1111/j.1439-0485.1989.tb00071.x

Hansen, C.D., MacEachern, J.A., 2007. Application of the asymmetric delta model to along-strike facies variations in a mixed wave- and river-influenced delta lobe, upper Cretaceous basal Belly River Formation, central Alberta, in: MacEachern, J. A. (Ed.) Applied Ichnology, SEPM. pp. 1–16.

Haq, B.U., 2014. Cretaceous eustasy revisited. Global and Planetary Change 113, 44–58. https://doi.org/10.1016/j.gloplacha.2013.12.007

Harder, H., 1980. Syntheses of Glauconite at Surface Temperatures. Clays and Clay Minerals 28, 217–222.

Hasegawa, H., Katsuta, N., Muraki, Y., Heimhofer, U., Ichinnorov, N., Asahi, H., Ando, H., Yamamoto, K., Murayama, M., Ohta, T., Yamamoto, M., Ikeda, M., Ishikawa, K., Kuma, R., Hasegawa, T., Hasebe, N., Nishimoto, S., Yamaguchi, K., Abe, F., Tada, R., Nakagawa, T., 2022. Decadal–centennial-scale solar-linked climate variations and millennial-scale internal oscillations during the Early Cretaceous. Scientific Reports 12, 21894. https://doi.org/10.1038/s41598-022-25815-w

Hay, W.W., DeConto, R.M., de Boer, P., Flögel, S., Song, Y., Stepashko, A., 2019. Possible solutions to several enigmas of Cretaceous climate. International Journal of Earth Sciences 108, 587–620. https://doi.org/10.1007/s00531-018-1670-2

Hay, W.W., Floegel, S., 2012. New thoughts about the Cretaceous climate and oceans. Earth-Science Reviews 115, 262–272. https://doi.org/10.1016/j.earscirev.2012.09.008

Hesser, T.J., Cialone, M.A., Anderson, M.E., 2013. Lake St. Clair: Storm Wave and Water Level Modeling. Engineer Research and Develpment Center, Vicksburg MS Coastal and Hydraulics Lab.

Hine, A., Martin, E., Jaeger, J., Brenner, M., 2017. Paleoclimate of Florida, in: Florida's Climate: Changes, Variations, & Impacts. Florida Climate Institute, pp. 457–484. https://doi.org/10.17125/fci2017.ch15

Hobday, David K., Morton, Robert A., Collins, Edward W., 1979. The Queen City Formation in the East Texas Embayment: a depositional record of riverine, tidal and wave interaction. The University of Texas at Austin, Bureau of Economic Geology, Geological Circular 80-4, 11p.

Hower, J., 1961. Some Factors Concerning the Nature and Origin of Glauconite. The American Mineralogist 46, 313–334.

Hubbard, S.M., Gingras, M.K., Pemberton, S.G., 2004. Palaeoenvironmental implications of trace fossils in estuary deposits of the Cretaceous Bluesky Formation, Cadotte region, Alberta, Canada. Fossils and Strata 51, 1-20.

Huck, S., Heimhofer, U., 2021. Early Cretaceous sea surface temperature evolution in subtropical shallow seas. Scientific Reports 11, 1–9. https://doi.org/10.1038/s41598-021-99094-2

Huck, S., Heimhofer, U., Immenhauser, A., Weissert, H., 2013. Carbon-isotope stratigraphy of Early Cretaceous (Urgonian) shoal-water deposits: Diachronous changes in

carbonate-platform production in the north-western Tethys. Sedimentary Geology 290, 157–174. https://doi.org/10.1016/j.sedgeo.2013.03.016

Hyžný, M., Šimo, V., Starek, D., 2015. Ghost shrimps (Decapoda: Axiidea: Callianassidae) as producers of an Upper Miocene trace fossil association from sublittoral deposits of Lake Pannon (Vienna Basin, Slovakia). Palaeogeography, Palaeoclimatology, Palaeoecology 425, 50–66. https://doi.org/10.1016/j.palaeo.2015.02.012

Immenhauser, A., 2005. High-rate sea-level change during the Mesozoic: New approaches to an old problem. Sedimentary Geology 175, 277–296. https://doi.org/10.1016/j.sedgeo.2004.12.016

Jafarzadeh, M., Tathagata, &, Choudhury, R., Taheri, A., Banerjee, S., Jafarian, A., 2020. Glauconite within Albian-Cenomanian Aitamir Formation, Kopet-Dagh Basin, northeastern Iran: origin and implications of Cretaceous seawater. Arabian Journal of Geosciences 13, 1236. https://doi.org/10.1007/s12517-020-05920-8/Published

Johnson, J.G., Murphy, M.A., 1984. Time-rock model for Siluro-Devonian continental shelf, western United States. Geological Society of America Bulletin 95, 1349–1359. https://doi.org/10.1130/0016-7606(1984)95<1349:TMFSCS>2.0.CO;2

Kelble, C.R., Johns, E.M., Nuttle, W.K., Lee, T.N., Smith, R.H., Ortner, P.B., 2007. Salinity patterns of Florida Bay. Estuarine, Coastal and Shelf Science 71, 318–334. https://doi.org/10.1016/j.ecss.2006.08.006

Kidwell, S.M., 1993. Taphonomic expressions of sedimentary hiatuses: field observations on bioclastic concentrations and sequence anatomy in low, moderate and high subsidence settings. Geologische Rundschau 82, 189–202.

Kier, P.M., 1962. Revision of the Cassiduloid Echinoids. Smithsonian Miscellaneous Collections 144, 1–262.

1292 Kjerfve, B., 1994. Chapter 1 Coastal Lagoons, in: Coastal Lagoon Processes, Elsevier
1293 Oceanography Series 60. Elsevier, pp. 1–8. https://doi.org/10.1016/S0422-9894(08)70006-
1294 0

1295 Komatsu, T., 1999. Depositional environments and bivalve fossil assemblages of the
1296 Lower Cretaceous Arida Formation, southwest Japan. The Journal of the Geological Society
1297 of Japan 105, 643–650.

1298 Komatsu, T., Chinzei, K., Zakhera, M.S., Matsuoka, H., 2002. Jurassic soft-bottom
1299 oyster *Crassostrea* from Japan. Palaeontology 45, 1037–1048.
1300 https://doi.org/10.1111/1475-4983.00274

1301 Komatsu, T., Maeda, H., 2005. Stratigraphy and fossil bivalve assemblages of the
1302 mid-Cretaceous Goshoura Group, southwest Japan. Paleontological Research 9, 119–142.

1303 Kondo, Y., Abbott, S.T., Kitamura, A., Kamp, P.J.J., Naish, T.R., Kamataki, T., Saul, G.S.,
1304 1998. The relationship between shellbed type and sequence architecture: examples from
1305 Japan and New Zealand. Sedimentary Geology 122, 109–127.
1306 https://doi.org/10.1016/S0037-0738(98)00101-8

1307 Kondo, Y., Kozai, T., Kikuchi, N., Sugawara, K., 2006. Ecologic and taxonomic
1308 diversification in the Mesozoic brackish-water bivalve faunas in Japan, with emphasis on
1309 infaunalization of heterodonts. Gondwana Research 10, 316–327.
1310 https://doi.org/10.1016/j.gr.2006.04.006

1311 Kosenko, I.N., 2014. On Late Jurassic and Early Cretaceous oysters (Bivalvia,
1312 Ostreidae) from northern Siberia. Paleontological Journal 48, 380–388.
1313 https://doi.org/10.1134/S003103011404008X

1314 Kroh, A., Nebelsick, J.H., 2003. Echinoid assemblages as a tool for
1315 palaeoenvironmental reconstruction - An example from the Early Miocene of Egypt.

Palaeogeography, Palaeoclimatology, Palaeoecology 201, 157–177. https://doi.org/10.1016/S0031-0182(03)00610-2

Kroth, M., Borghi, L., Bobco, F.E.R., Araújo, B.C., Silveira, L.F., Duarte, G., Ferreira, L.D.O., Guerra-Sommer, M., Mendonça, J.D.O., 2021. Aptian shell beds from the Romualdo Formation (Araripe Basin): Implications for paleoenvironment and paleogeographical reconstruction of the Northeast of Brazil. Sedimentary Geology 426, 106025. https://doi.org/10.1016/j.sedgeo.2021.106025

Laita, E., Bauluz, B., Aurell, M., Bádenas, B., Canudo, J.I., Yuste, A., 2020. A change from warm/humid to cold/dry climate conditions recorded in lower Barremian clay-dominated continental successions from the SE Iberian Chain (NE Spain). Sedimentary Geology 403, 105673. https://doi.org/10.1016/j.sedgeo.2020.105673

Lazo, D.G., 2004. Análisis de concentraciones fósiles del Cretácico Inferior de la Cuenca Neuquina. PhD Thesis. Universidad de Buenos Aires.

Lazo, D.G., 2007a. Early Cretaceous bivalves of the Neuquén Basin, west-central Argentina: notes on taxonomy, palaeobiogeography and palaeoecology. Geological Journal 42, 127–142.

Lazo, D.G., 2007b. Análisis de biofacies y cambios relativos del nivel del mar en el Miembro Pilmatué de la Formación Agrio, Cretácico Inferior de cuenca Neuquina, Argentina. Ameghiniana 44, 73–89.

Lazo, D.G., Aguirre-Urreta, M.B., Price, G.D., Rawson, P.F., Ruffell, A.H., Ogle, N., 2008. Palaeosalinity variations in the Early Cretaceous of the Neuquén Basin, Argentina: Evidence from oxygen isotopes and palaeoecological analysis. Palaeogeography, Palaeoclimatology, Palaeoecology 260, 477–493. https://doi.org/10.1016/j.palaeo.2007.12.008

Mallada, L., 1878. Sinopsis de las especies fósiles que se han encontrado en España. Madrid. Imprenta y Fundición de M. Tello, Impresor de Cámara de Su Majestad, Madrid.

Marin, P., Sornay, J., 1971. Précisions sur l'âge des formations aptiennes aux confins de l'Aragón et du Maestrazgo (Provinces de Teruel et Castellón de la Plana, Espagne). Compte Rendu Sommaire des Séances de la Société Géologique de France, 165–167.

Martín-Chivelet, J., López-Gómez, J., Aguado, R., Arias, C., Arribas, J., Arribas, M.E., Aurell, M., Bádenas, B., Benito, M.I., Bover-Arnal, T., Casas Sáinz, A., Castro, J.M., Coruña, F., de Gea, G.A., Fornós, J.J., Fregenal-Martínez, M., García-Senz, J., Garófano, D., Gelabert, B., Giménez, J., González-Acebrón, L., Guimerà, J., Liesa, C.L., Mas, R., Meléndez, N., Molina, J.M., Muñoz, J.A., Navarrete, R., Nebot, M., Nieto, L.M., Omodeo-Salé, S., Pedrera, A., Peropadre, C., Quijada, I.E., Quijano, M.L., Reolid, M., Robador, A., Rodríguez-López, J.P., Rodríguez-Perea, A., Rosales, I., Ruiz-Ortiz, P.A., Sàbat, F., Salas, R., Soria, A.R., Suarez-Gonzalez, P., Vilas, L., 2019. The Late Jurassic-Early Cretaceous Rifting, in: Quesada, C., Oliveira, J.T (Eds.), 2019. The Geology of Iberia: A Geodynamic Approach. Volume 3: The Alpine Cycle. Springer, Berlin, pp. 169–251.

Martínez, R., Grauges, A., Salas, R., 1994. Distribución de los ammonites del Cretácico inferior de la Cordillera Costera Catalana e Ibérica Oriental. Cuadernos de Geología Ibérica 18, 337–354. https://doi.org/10.5209/rev_CGIB.1994.v18.2583

McConchie, D.M., Ward, J.B., McCann, V.H., Lewis, D.W., 1979. A Mössbauer Investigation of Glauconite and its Geological Significance. Clays and Clay Minerals. 27, 339–348. https://doi.org/10.1346/CCMN.1979.0270504

Mendoza, O., Pretell, K., Diringer, B., Avellan, R., Zapata, K., Marchan, A., Cedeño, V., Peralta, T., Ordinola, A., Mialhe, E., 2017. Respuesta fisiológica y molecular de *Anadara tuberculosa* (Arcoida: Arcidae) al estrés de salinidad. Revista de Biología Tropical 65 (3), 1142-1151.

Moreno Bedmar, J.-A., 2007. Precisiones sobre la edad, mediante ammonoideos y nautiloideos, de la Fm. Margas del Forcall en la subcuenca de Oliete (Cadena Ibérica, España). Geogaceta 75–78.

Moreno-Bedmar, J.A., Company, M., Bover-Arnal, T., Salas, R., Delanoy, G., Martínez, R., Grauges, A., 2009. Biostratigraphic characterization by means of ammonoids of the lower Aptian Oceanic Anoxic Event (OAE 1a) in the eastern Iberian Chain (Maestrat Basin, eastern Spain). Cretaceous Research 30, 864–872. https://doi.org/10.1016/j.cretres.2009.02.004

Moreno-Bedmar, J.A., Company, M., Bover-Arnal, T., Salas, R., Delanoy, G., Maurrasse, F.J.M.R., Grauges, A., Martínez, R., 2010. Lower Aptian ammonite biostratigraphy in the Maestrat Basin (Eastern Iberian Chain, Eastern Spain). A Tethyan transgressive record enhanced by synrift subsidence. Geologica Acta 8, 281–299. https://doi.org/10.1344/105.000001534

Morris, R.L., Bilkovic, D.M., Boswell, M.K., Bushek, D., Cebrian, J., Goff, J., Kibler, K.M., La Peyre, M.K., McClenachan, G., Moody, J., Sacks, P., Shinn, J.P., Sparks, E.L., Temple, N.A., Walters, L.J., Webb, B.M., Swearer, S.E., 2019. The application of oyster reefs in shoreline protection: Are we over-engineering for an ecosystem engineer? Journal of Applied Ecology 56, 1703–1711. https://doi.org/10.1111/1365-2664.13390

Moss, S., Tucker, M.E., 1995. Diagenesis of Barremian-Aptian platform carbonates (the Urgonian Limestone Formation of SE France): near-surface and shallow-burial diagenesis. Sedimentology 42, 853–874. https://doi.org/10.1111/j.1365-3091.1995.tb00414.x

Mulder, T., Alexander, J., 2001. The physical character of subaqueous sedimentary density flow and their deposits. Sedimentology 48, 269–299. https://doi.org/10.1046/j.1365-3091.2001.00360.x

Murat, B., 1983. Contribution à l'étude stratigraphique, sédimentologique et tectonique du Bassin Éocrétacé d'Oliete (Provinde de Teruel, Espagne). PhD Thesis, Université Paul Sabatier (Toulouse).

Murphy, M.A., Salvador, A., 1999. International stratigraphic guide - An abridged version. Episodes 22, 255–271.

Nakano, T., Sasaki, T., 2011. Recent advances in molecular phylogeny, systematics and evolution of patellogastropod limpets. Journal of Molluscan Studies 77, 203–217. https://doi.org/10.1093/mollus/eyr016

Olariu, C., Steel, R.J., Dalrymple, R.W., Gingras, M.K., 2012. Tidal dunes versus tidal bars: The sedimentological and architectural characteristics of compound dunes in a tidal seaway, the lower Baronia Sandstone (Lower Eocene), Ager Basin, Spain. Sedimentary Geology 279, 134–155. https://doi.org/10.1016/j.sedgeo.2012.07.018

Pemberton, S.G., MacEachern, J., Frey, R.W., 1992. Trace fossil facies models: Environmental and allostratigraphic significance, in: Walker, R.G., James, N.P. (Eds.) (1992). Facies Models: Response to Sea Level Change. Geological Association of Canada, pp. 47–72.

Pemberton, S.G., MacEachern, J.A., Dashtgard, S.E., Bann, K.L., Gingras, M.K., Zonneveld, J.P., 2012. Shorefaces, in: Developments in Sedimentology. Elsevier B.V., pp. 563–603. https://doi.org/10.1016/B978-0-444-53813-0.00019-8

Peropadre, C., 2011. El Aptiense del margen occidental de la Cuenca del Maestrazgo: controles tectónico, eustático y climático en la sedimentación. PhD Tesis, Universidad Complutense de Madrid.

Peropadre, C., Meléndez, N., Liesa, C.L., 2007. Heterogeneous subsidence and paleogeographic elements in an extensional setting revealed through the correlation of a storm deposit unit (Aptian, E Spain). Journal of Iberian Geology 33, 79–91.

1414 Petuch, E.J., 2004. Cenozoic seas: the view from eastern North America. CRC Press,
1415 Boca Raton, 308p.

1416 Petuch, E.J., Berschauer, D.P., 2022. Mollusks and Marine Environments of the Ten
1417 Thousand Islands, 1st ed. CRC Press, Boca Raton, 157p.
1418 https://doi.org/10.1201/9781003309949

1419 Peyrot, D., Rodríguez-López, J.P., Lassaletta, L., Meléndez, N., Barrón, E., 2007.
1420 Contributions to the palaeoenvironmental knowledge of the Escucha Formation in the
1421 Lower Cretaceous Oliete Sub-basin, Teruel, Spain. Comptes Rendus - Palevol 6, 469–481.
1422 https://doi.org/10.1016/j.crpv.2007.09.014

1423 Pittet, B., Van Buchem, F.S.P., Hillgärtner, H., Razin, P., Grötsch, J., Droste, H., 2002.
1424 Ecological succession, palaeoenvironmental change, and depositional sequences of
1425 Barremian-Aptian shallow-water carbonates in northern Oman. Sedimentology 49, 555–
1426 581. https://doi.org/10.1046/j.1365-3091.2002.00460.x

1427 Pollard, J.E., Goldring, R., Buck, S.G., 1993. Ichnofabrics containing *Ophiomorpha*:
1428 significance in shallow-water facies interpretation. Journal of the Geological Society 150,
1429 149–164. https://doi.org/10.1144/gsjgs.150.1.0149

1430 Pourmozaffar, S., Tamadoni Jahromi, S., Rameshi, H., Sadeghi, A., Bagheri, T.,
1431 Behzadi, S., Gozari, M., Zahedi, M.R., Abrari Lazarjani, S., 2020. The role of salinity in
1432 physiological responses of bivalves. Reviews in Aquaculture 12, 1548–1566.
1433 https://doi.org/10.1111/raq.12397

1434 Radley, J.D., Allen, P., 2012. The Wealden (non-marine Lower Cretaceous) of the
1435 Wessex Sub-basin, southern England. Proceedings of the Geologists' Association 123, 319–
1436 373. https://doi.org/10.1016/j.pgeola.2012.01.002

Radley, J.D., Barker, M.J., 1998. Stratigraphy, palaeontology and correlation of the Vectis Formation (Wealden Group, Lower Cretaceous) at Compton Bay, Isle of Wight, southern England. Proceedings of the Geologists' Association 109, 187–195. https://doi.org/10.1016/S0016-7878(98)80065-5

Radley, J.D., Barker, M.J., 1998. Stratigraphy, palaeontology and correlation of the Vectis Formation (Wealden Group, Lower Cretaceous) at Compton Bay, Isle of Wight, southern England. Proceedings of the Geologists' Association 109, 187–195. https://doi.org/10.1016/S0016-7878(98)80065-5

Radley, J.D., Barker, M.J., 2000. Palaeoenvironmental significance of storm coquinas in a Lower Cretaceous coastal lagoonal succession (Vectis Formation, Isle of Wight, southern England). Geological Magazine 137, 193–205. https://doi.org/10.1017/S0016756800003782

Rahiminejad, A.H., Hassani, M.J., 2016. Paleoenvironmental distribution patterns of orbitolinids in the Lower Cretaceous deposits of eastern Rafsanjan, Central Iran. Marine Micropaleontology 122, 53–66. https://doi.org/10.1016/j.marmicro.2015.11.006

Rakshit, S., Dale, A.W., Wallace, D.W., Algar, C.K., 2023. Sources and sinks of bottom water oxygen in a seasonally hypoxic fjord. Frontiers in Marine Science 10, 1148091. https://doi.org/10.3389/fmars.2023.1148091

Reboulet, S., Szives, O., Aguirre-Urreta, B., Barragán, R., Company, M., Frau, C., Kakabadze, M.V., Klein, J., Moreno-Bedmar, J.A., Lukeneder, A., Pictet, A., Ploch, I., Raisossadat, S.N., Vašíček, Z., Baraboshkin, E.J., Mitta, V.V., 2018. Report on the 6th International Meeting of the IUGS Lower Cretaceous Ammonite Working Group, the Kilian Group (Vienna, Austria, 20th August 2017). Cretaceous Research 91, 100–110. https://doi.org/10.1016/j.cretres.2018.05.008

Rigaud, S., Deflandre, B., Grenz, C., Cesbron, F., Pozzato, L., Voltz, B., Grémare, A., Romero-Ramirez, A., Mirleau, P., Meulé, S., Faure, V., Mayot, N., Michotey, V., Bonin, P., Pascal, L., Cordier, M.-A., Lamarque, B., Tenório, M., Radakovitch, O., 2021. Benthic oxygen dynamics and implication for the maintenance of chronic hypoxia and ecosystem degradation in the Berre lagoon (France). Estuarine, Coastal and Shelf Science 258, 107437. https://doi.org/10.1016/j.ecss.2021.107437

Rodríguez-López, J.P., Liesa, C.L., Meléndez, N., Soria, A.R., 2007. Normal fault development in a sedimentary succession with multiple detachment levels: The Lower Cretaceous Oliete sub-basin, Eastern Spain. Basin Research 19, 409–435. https://doi.org/10.1111/j.1365-2117.2007.00327.x

Scholle, P.A., Ulmer-Scholle, D., 2003. A Color Guide to the Petrography of Carbonate Rocks: Grains, Textures, Porosity, Diagenesis, AAPG Memoir, 77, 474p.. The American Association of Petroleum Geologists, Tulsa.

Semeniuk, V., 1971. Suaberial leaching in the limestones of the Bowan Park Group (Ordovician) of central western New South Wales. Journal of Sedimentary Petrology 41, 939–950.

Shanmugam, G., 2018. The hyperpycnite problem. Journal of Palaeogeography 7, 1–42. https://doi.org/10.1186/s42501-018-0001-7

Simón, J.L., Liesa, C.L., 2011. Incremental slip history of a thrust: Diverse transport directions and internal folding of the Utrillas thrust sheet (NE Iberian Chain, Spain). Geological Society Special Publications 349, 77–97. https://doi.org/10.1144/SP349.5

Soderqvist, L.E., Patino, E., 2010. Seasonal and Spatial Distribution of Freshwater Flow and Salinity in the Ten Thousand Islands Estuary, Florida, 2007–2009, U.S. Geological Survey Data Series 501, 54p.

Soria, A.R., Martin-Closas, C., Melendez, A., Melendez, M.N., Aurell, M., 1995. Estratigrafia del Cretacico inferior continental de la Cordillera Iberica Central. Estudios Geologicos 51, 141–152.

Soria, A.R., Vennin, E., Meléndez, A., 1994. Estratigrafía, sedimentología y control tectónico en la evolución de las rampas carbonatadas del Cretácico Inferior de la Cubeta de Oliete (provincia de Teruel). Revista de la Sociedad Geologica de España 7, 47–61.

Sornay, J., Marin, P., 1972. Sur la faune d'ammonites aptiennes de la Tejeria de Josa (Teruel, Espagne). Annales de Paléontologie 63, 101–123.

Stanley, S.S., 1970. Relation of Shell Form to Life Habits of the Bivalvia (Mollusca), in: GSA Memoirs 125, 1–282.

Stehli, F.G., Hower, J., 1961. Mineralogy and early diagenesis of carbonate sediments. Journal of Sedimentary Research 31, 358–371. https://doi.org/10.1306/74D70B7D-2B21-11D7-8648000102C1865D

Stenzel, H.B., 1971. Mollusca 6: Bivalvia: Oysters, in: Stenzel, H.B. (Ed.), Treatise on Invertebrate Paleontology. The Geological Society of America, Lawrence, pp. 953–1224.

Ten Hove, H.A., Van Den Hurk, P., 1993. A review of recent and fossil serpulid "reefs'; actuopalaeontology and the "Upper Malm' serpulid limestones in NW Germany. Geologie en Mijnbouw 72, 23–67.

Toulouse, D., 1971. Contribution à la connaissance géologique de la région d'Oliete (Province de Teruel - Espagne). PhD Thesis, Université de Dijon.

Veiga, G.D., Schwarz, E., Spalletti, L.A., Massaferro, J.L., 2013. Anatomy and sequence architecture of the early post-rift in the Neuquén Basin (Argentina): A response to physiography and relative sea-level changes. Journal of Sedimentary Research 83, 746–765. https://doi.org/10.2110/jsr.2013.56

1509 Vennin, E., Aurell, M., 2001. Stratigraphie sequentielle de l'Aptien du sous-bassin de
1510 Galve (Province de Teruel, NE de l'Espagne). Bulletin de la Société Géologique de France 172,
1511 397–410. https://doi.org/10.2113/172.4.397

1512 Vennin, E., Soria de Miguel, A., Preat, A., Meléndez Hevia, A., 1993. Análisis
1513 secuencial durante el intervalo Barremiense-Aptiense en la Cubeta de Oliete. Cuadernos de
1514 Geología Ibérica 257–283. https://doi.org/10.5209/rev_CGIB.1993.v17.2599

1515 Waite, R., Allmon, W.D., 2016. Observations on the Biology and Sclerochronology of
1516 *"Turritella" duplicata* (Linnaeus, 1758) (Cerithioidea, Turritellidae) from Southern Thailand.
1517 Malacologia 59, 247–269. https://doi.org/10.4002/040.059.0206

1518 Walker, R.G., James, N.P., 1992. Facies Models: Response to Sea Level Change.
1519 Geological Association of Canada, St Johns.

1520 Winsemann, J., Lang, J., Fedele, J.J., Zavala, C., Hoyal, D.C.J.D., 2021. Re-examining
1521 models of shallow-water deltas: Insights from tank experiments and field examples.
1522 Sedimentary Geology 421, 105962. https://doi.org/10.1016/j.sedgeo.2021.105962

1523 Witzke, B.J., 1987. Models for circulation patterns in epicontinental seas applied to
1524 Paleozoic facies of North America craton. Paleoceanography 2, 229–248.
1525 https://doi.org/10.1029/PA002i002p00229

1526 Woodin, S.A., Wethey, D.S., Olabarria, C., Vázquez, E., Domínguez, R., Macho, G.,
1527 Peteiro, L., 2020. Behavioral responses of three venerid bivalves to fluctuating salinity stress.
1528 Journal of Experimental Marine Biology and Ecology 522, 151256.
1529 https://doi.org/10.1016/j.jembe.2019.151256

1530 Wright, V.P., Burgess, P.M., 2005. The carbonate factory continuum, facies mosaics
1531 and microfacies: an appraisal of some of the key concepts underpinning carbonate
1532 sedimentology. Facies 51, 17–23. https://doi.org/10.1007/s10347-005-0049-6

1533 Xia, M., Jiang, L., 2015. Influence of wind and river discharge on the hypoxia in a
1534 shallow bay. Ocean Dynamics 65, 665–678. https://doi.org/10.1007/s10236-015-0826-x

1535 Yin, J., Fürsich, F.T., Werner, W., 1995. Reconstruction of palaeosalinity using carbon
1536 isotopes and benthic associations: a comparison. Geologische Rundschau 84, 223–236.
1537 https://doi.org/10.1007/BF00260436

1538 Zavala, C., 2020. Hyperpycnal (over density) flows and deposits. Journal of
1539 Palaeogeography, 9 (17), 1-21. https://doi.org/10.1186/s42501-020-00065-x

1540 Zavala, C., Arcuri, M., Blanco Valiente, L., 2012. The importance of plant remains as
1541 a diagnostic criteria for the recognition of ancient hyperpycnites. Revue de Paléobiologie 11,
1542 457–469.

1543 Zecchin, M., Caffau, M., Catuneanu, O., Lenaz, D., 2017. Discrimination between
1544 wave-ravinement surfaces and bedset boundaries in Pliocene shallow-marine deposits,
1545 Crotone Basin, southern Italy: An integrated sedimentological, micropalaeontological and
1546 mineralogical approach. Sedimentology 64, 1755–1791. https://doi.org/10.1111/sed.12373

1547 Zecchin, M., Catuneanu, O., Caffau, M., 2019. Wave-ravinement surfaces:
1548 Classification and key characteristics. Earth-Science Reviews 188, 210–239.
1549 https://doi.org/10.1016/j.earscirev.2018.11.011

1550 Zinke, J., Reijmer, J.J.G., Taviani, M., Dullo, W.C., Thomassin, B., 2005. Facies and
1551 faunal assemblage changes in response to the Holocene transgression in the Lagoon of
1552 Mayotte (Comoro Archipelago, SW Indian Ocean). Facies 50, 391–408.
1553 https://doi.org/10.1007/s10347-004-0040-7

1554

1555 **Fig. 1 A.** Position of Iberia within the Western Tethys during the Early Aptian, showing the
1556 approximate boundary between northern hemisphere humid and arid climatic belts. Modified

from Steuber et al. (2005) and Chumakov et al. (2005). **B.** Distribution of subbasins within the Maestrazgo Basin (Mb): Ol: Oliete; Mo: Morella; Per: Perellò; Pa: Las Parras; Ga: Galve; Pen: Penyagolosa; Sa: Salzedella. **C.** Geological map of the Oliete subbasin showing the logged locations and control points. The inset shows the chronostratigraphic distribution of the Barremian-Albian units of the Oliete subbasin. Slightly modified from García-Penas et al. (2022).

Fig. 2 A. Intercalations of siltstone beds between the basal clays of the lower Tejería Fm (F1). **B.** Fine-grained sandstone bed with hummocky cross-stratification (F4) intercalated in the basal clays of the Josa Fm, Ariño (Fig. 1C). **C.** Detail view of poorly lithified sandstone with abundant *Palorbitolina* and solitary corals (F9) found in the middle part of the Josa Fm, Alacón (Fig. 1C, 2). **D.** Articulated internal moulds of bivalves and gastropods floating in a micritic matrix (F10). Sequence O2 in Estercuel. **E.** Abraded internal mould of a bivalve colonised by an epibenthic limpet. Sequence O2, Ariño. **F.** Articulated oyster and serpulid aggregations in a white micritic matrix (F11a), Cabezo Negro. **G.** Bouquet-shaped aggregation of *Crassostrea* sp. (F11a) in Sequence O2 in Estercuel. Length of pen: 15cm. **H.** Turriculate gastropod floatstone (F10). Upper part of sequence O2, Blesa. Diameter of lens cap: 4cm. **I.** Mud-supported limestone with abundant *Thalassinoides* isp. burrows. Basal part of Sequence O2, Ariño. **J.** Poorly-lithified cross-laminated unfossiliferous sandstone with intercalations of heterolithic sand-silt alternations (white rectangle). Uppermost sequence O2, Blesa. White rectangle shows location of Fig. 10N. Scale measures 15 cm. **K.** Interpretation of J. **L.** Bioclastic hummocky cross-stratified limestone in the uppermost part of sequence J, at control point 4. **M.** Coal-bearing clay and sandstone beds of the lower Escucha Fm overlying the topmost Oliete Fm at control point 10, near Berge. **N.** Detail view of heterolithic sand-silt lamination in the uppermost part of Sequence O2, Blesa. Length of pen: 15cm.

Fig. 3 Correlation of three representative logs of the Josa Fm, showing the identified facies, discontinuities, and transgressive-regressive trends, as well as percentages of $CaCO_3$ in the logs of Alacón and Tejería de Josa.

Fig. 4 A. Fine sandstone (Facies 3), interpreted as hyperpycnal flow deposit. Note the fine grain size, good sorting and presence of opaque organic (probably plant) debris (white arrows). **B.** Sandstone containing abundant broken and rounded oyster fragments (white arrows) (Facies 6a). **C.** Sandy limestone containing mostly fragments of oysters and gastropods (white arrows) (Facies 5). **D.** Orbitolinid sandstone (Facies 9). Note the predominance of flattened orbitolinids and the occurrence of bryozoans (white arrow). **E.** Bivalve-gastropod floatstone (Facies 10), gastropod shells of various sizes in a wackestone matrix with abundant bioclasts of thin-shelled bivalves, gastropods, oysters, ostracods and rare green algae (white arrows). **F.** Sponge spiculite containing crustacean microcoprolites (white arrows), flat micritic pebbles and disarticulated echinoderm elements. **G:** Bioclastic packstone (Facies 12) containing abundant debris of bivalves, gastropods, ostracods, serpulids and echinoderms. **H.** Bioturbated peloidal-bioclastic grainstone (Facies 13). **I.** Cortoidal grainstone (Facies 14) with abundant bioclasts of green algae, gastropods, bivalves and ostracods, as well as benthic foraminifera (e.g. white arrows). **J.** Peloidal-bioclastic grainstone (Facies 15) containing abundant small gastropods. **K.** Bioclastic-cortoidal grainstone with opaque iron ooids (Facies 16). Concentric banding can be observed in the thinner-cut lower part of the thin section (white arrows). **L.** Intraclastic grainstone (Facies 17).

Fig. 5 A. Isopach map of sequence J, including a simplified view of the major fault systems controlling deposition in the Oliete Subbasin during the Aptian. The reconstructed Cenozoic displacement of the Utrillas Fault System (Simón and Liesa, 2011) is represented with a dotted orange line. **B.** Combined isopach map of sequences O1-O3, showing all logged localities and

control points used in this study. Grey areas (in both maps) show the extent of total or partial Cenozoic erosion of the studied succession.

Fig. 6 Fence diagram showing the facies distribution and thickness of sequence J. The location of individual logs is shown in Fig. 1C. Map shows the extent of the transects over the Oliete subbasin.

Fig. 7 A. Panoramic view of mixed carbonate-siliciclastic units with planar cross-stratification topping sequence J at Alacón (Fig. 1C). Note the bimodal distribution of palaeocurrents (yellow and red arrows). **B.** Sequence O1 at control point 2, near Alcaine. Note the presence of cross-stratified beds with convex top surfaces at the top of the sequence. **C.** Panoramic view of Sequence J at Ariño. Note the presence of a lobate unit of Facies 17 in the upper part of the sequence.

Fig. 8 Idealised palaeoenvironmental reconstruction of the northwestern margin of the Maestrazgo Basin. Areas adjacent to the Oliete Subbasin have been reconstructed based on new field work (control points 8, 9, 12 in Fig. 1) and previous reconstructions by Peropadre (2011) and Clariana (1999). All stages represent the idealised palaeoenvironmental distribution during the regressive stage of each sequence, based on the correlation of all available logs and observations at control points (Fig. 1). **A.** Simplified distribution of sedimentary domains and palaeoenvironments in the Maestrazgo Basin during the Aptian. The black rectangle indicates the area represented in B-E. **B.** Palaeoenvironmental distribution of the Oliete Subbasin during sequence J. Note the inferred position of a small deltaic body between the localities of Josa and Obón, and the development of storm-influenced large-scale dunes in the northwestern area of the subbasin. **C.** Palaeoenvironmental distribution during sequence O1. Note the development of storm-generated bioclastic lobes (see also Fig. 7B) at the western margin of the subbasin. **D.** Palaeoenvironmental distribution of sequence O2. Note the extent of siliciclastic peritidal environments at the western margin of the subbasin. **E.** Palaeoenvironmental distribution

during sequence O3. Note the development of peloidal facies and large-scale storm-influenced bedforms at the northwestern margin of the subbasin. A deeper seaway between the Oliete and Las Parras subbasins is inferred to have existed at this stage, allowing better marine circulation and an increase in environmental energy.

Fig. 9 Correlation of three representative logs of the Oliete Fm, showing the identified facies, discontinuities, and transgressive-regressive trends, as well as percentages of $CaCO_3$ in the logs of Alacón and Estercuel.

Fig. 10 Fence diagram showing the thickness and facies distribution of sequences O1-O3 across the Oliete subbasin. The location of individual logs is shown in Fig. 1C. Map shows the extent of the transects over the Oliete subbasin.

Fig. 11 A. View of discontinuity B1 at the top of the Alacón Fm in Blesa, showing karstification (bivalve borings enlarged by dissolution) and iron-staining. Person for scale is 180 cm tall. **B.** Detail of discontinuity O1 showing a cemented oyster in a karst cavity. **C.** Detail view of discontinuity surface B1.1, showing abundant bivalve borings and iron staining. **D.** Bottom view of the topmost beds of sequence J at Alcaine, immediately below discontinuity B2, showing abundant *Thalassinoides* isp. bioturbation. **E.** Discontinuity B3 at Cabezo Negro (Fig. 1C, 3), showing epikarst features with a reddish clay infill. **F.** Discontinuity B4 at control point 3 near Oliete, expressed as an irregular iron-stained surface developed on bioclastic limestone, and overlain by peloidal limestones with abundant *Thalassinoides* isp. bioturbation and mass accumulations of glauconite. **G.** Polished slab of the mass-accumulations of glauconite immediately overlying discontinuity B4 in Estercuel. Note the presence of white micritic clasts and abundant oyster fragments. **H.** Detail view of discontinuity B5 at control point 4, showing epikarst features with a reddish clay infill. **I.** Panoramic view of discontinuity B5 topping the whitish peloidal limestones of the uppermost Oliete Fm, and overlain by the ochre sandstones and clays of the lowermost Escucha Fm. Person for scale (white arrow) is ca. 175 cm tall.

Fig. 12 A. Panoramic view of the Josa Fm at the Tejería de Josa outcrop (TJ log, Fig. 1C, 3). Note the thickening-up stacking of strata. **B.** Panoramic view of the Josa and Oliete formations in Alcaine, pointing out the main transgressive-regressive sequences (J SO1-SO3) and discontinuities (B1-B5). **C.** Panoramic view of the studied interval in control point 10, near Berge (Fig. 1C). The transgressive clays of the Josa Fm (i.e of Sequence J) are overlain by an abnormally thick ochre cross-stratified interval, which is interpreted as a condensed lateral equivalent of at least part of sequences O1-O3. The white frame indicates the location of Fig. 2M. Note also the folded and tilted Lower Jurassic succession underlying the Aptian units.

Fig. 13 A. Discontinuity B2 topping the Josa Fm at Tejería de Josa (Fig 1C), expressed as an irregular surface of a medium-grained cross-stratified sandstone unit, overlain by a shell bed. **B.** Detail view of discontinuity B2 and its associated shell bed. Note the well-developed ferruginous crust underlying the shell bed, and the presence of *Skolithos* isp. in the underlying bed of sequence J. Diameter of lens cap: 4 cm. **C.** Detail view of discontinuity B2 near Oliete (Fig 1C), expressed as an irregular iron-stained surface with abundant bivalve borings. **D.** Detail view of discontinuity B2 in the Alacón log, overlain by a shell bed. Note the presence of iron-stained surfaces topping B2 and the overlying shell bed. **E.** Discontinuity B2 in Alacón. The overlying shell bed has been eroded away, exposing the upper iron-stained surface of B2. Note the cut-off articulated bivalves, evidencing a certain amount of abrasion associated with discontinuity B2. **F.** Polished slab of the shell bed overlying discontinuity B2. Note the micritic clasts in the lower part, and of shell fragments and encrusting serpulids towards the top, as well as the upwards-increasing iron staining. **G.** Thin section of the shell bed overlying discontinuity B2. Note the abundance of fine quartz sand, serpulids, small abraded shell fragments, phosphatic grains (white arrows) and pervasive opaque iron staining.

Fig. 14 Relative abundances of key faunal groups across the main identified palaeoenvironments and their corresponding facies associations. Colours follow the pattern of Fig. 8.

1679

1680 **Table 1** Key features of the Josa Formation defined in this work.

1681 **Table 2** Detailed features of the 17 lithofacies defined in the Josa and Oliete formations.

- The detailed sedimentary evolution of a marginal-marine bay is presented.
- Four T-R sequences are bounded by maximum regressive surfaces.
- Faunal associations are put in a sequence-stratigraphic context.
- Massive glauconite accumulations in intertidal to lagoonal settings.

Figure 1

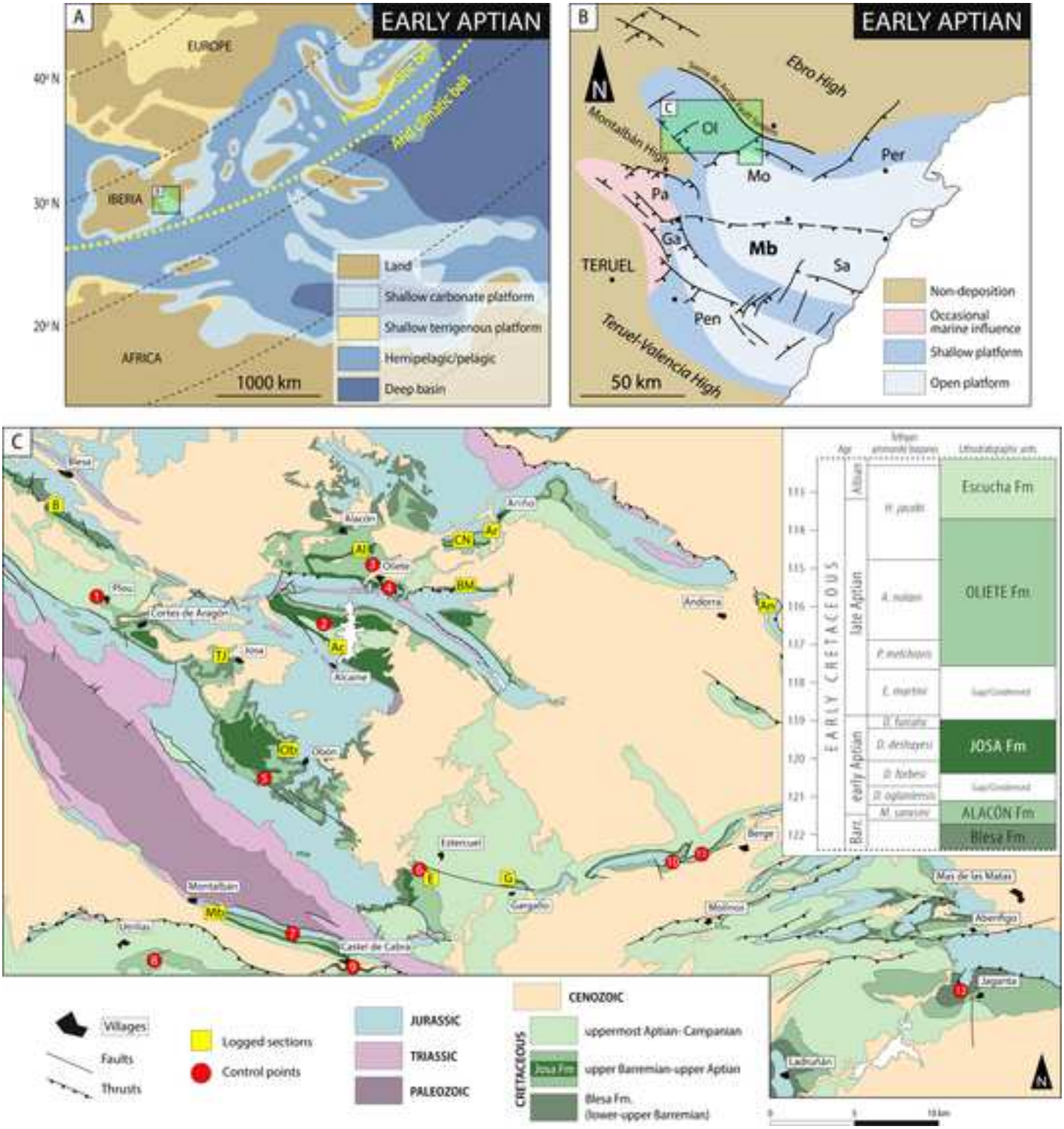

Figure 2

Click here to access/download;Figure;Fig.2.tif

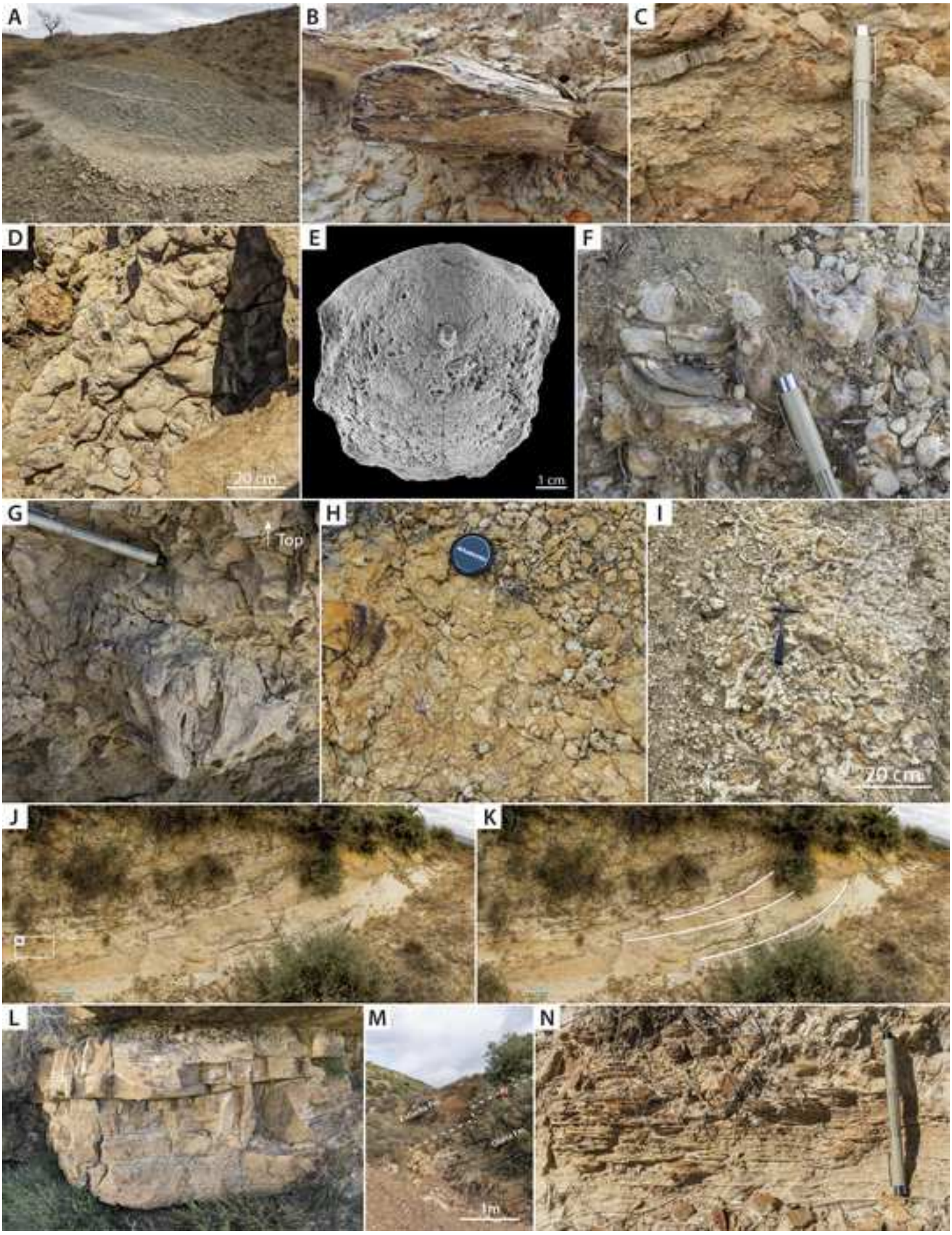

Figure 3

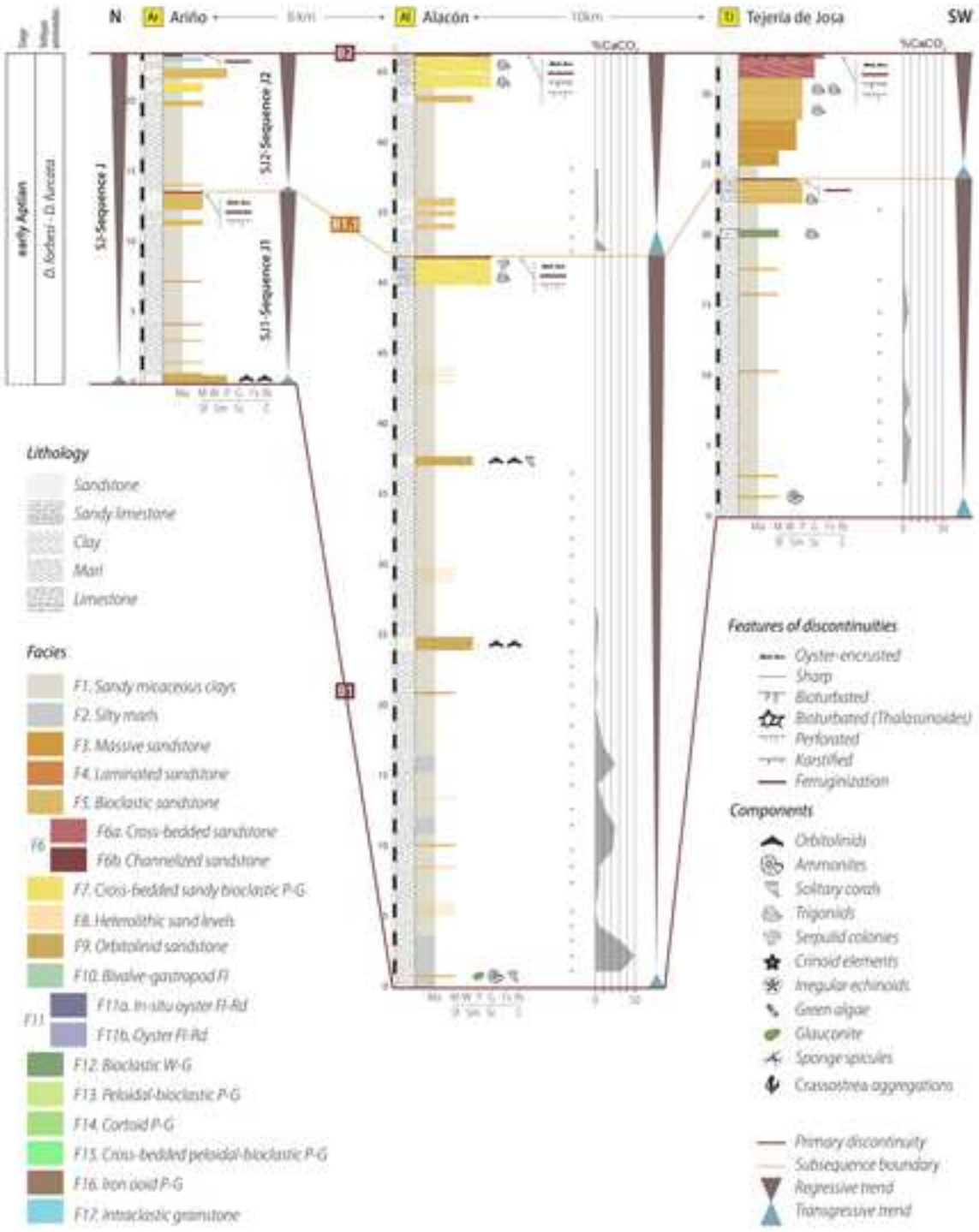

Figure 4

Click here to access/download;Figure;Fig.4.tif

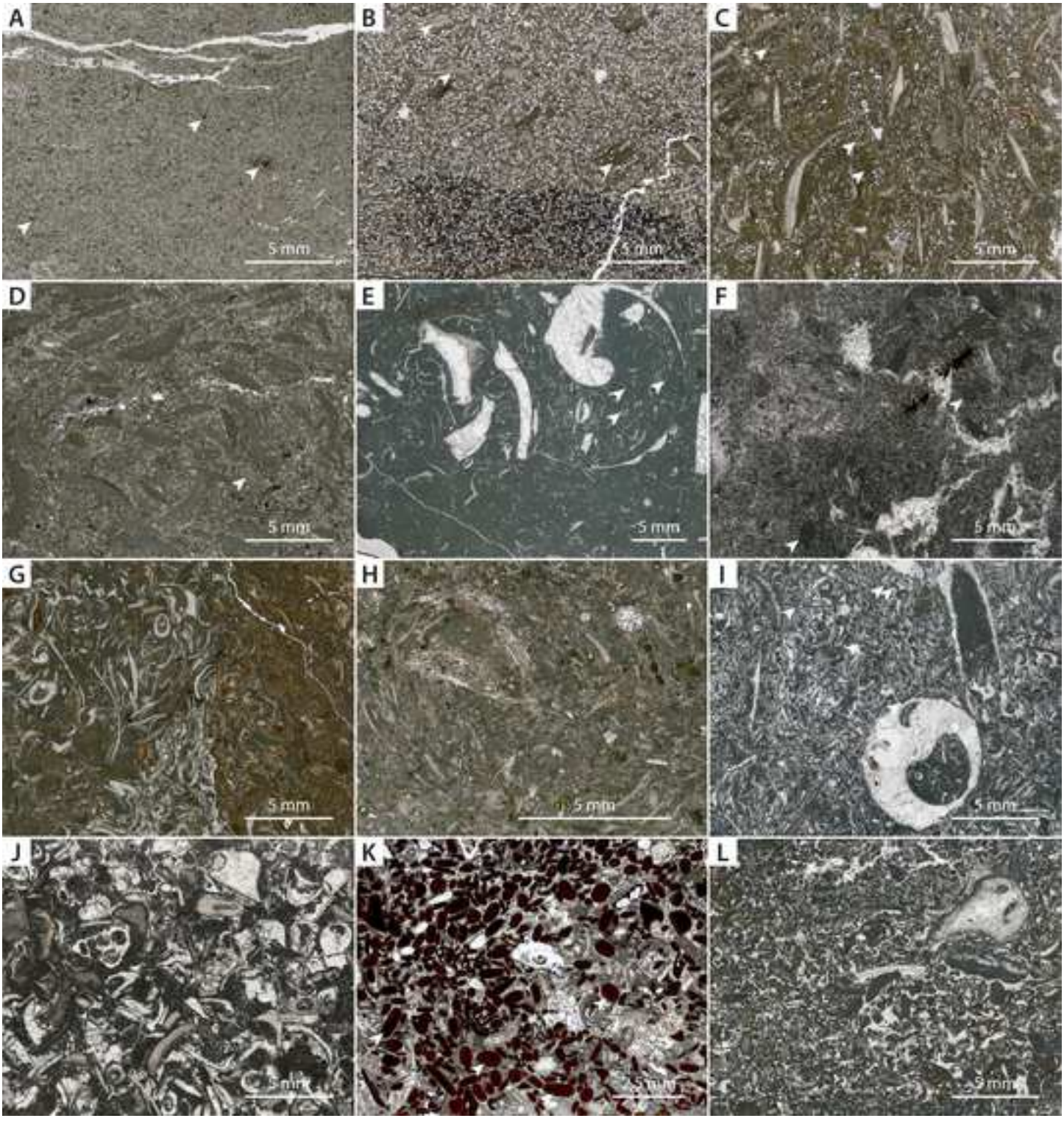

Figure 5

Click here to access/download;Figure;Fig.5.tif

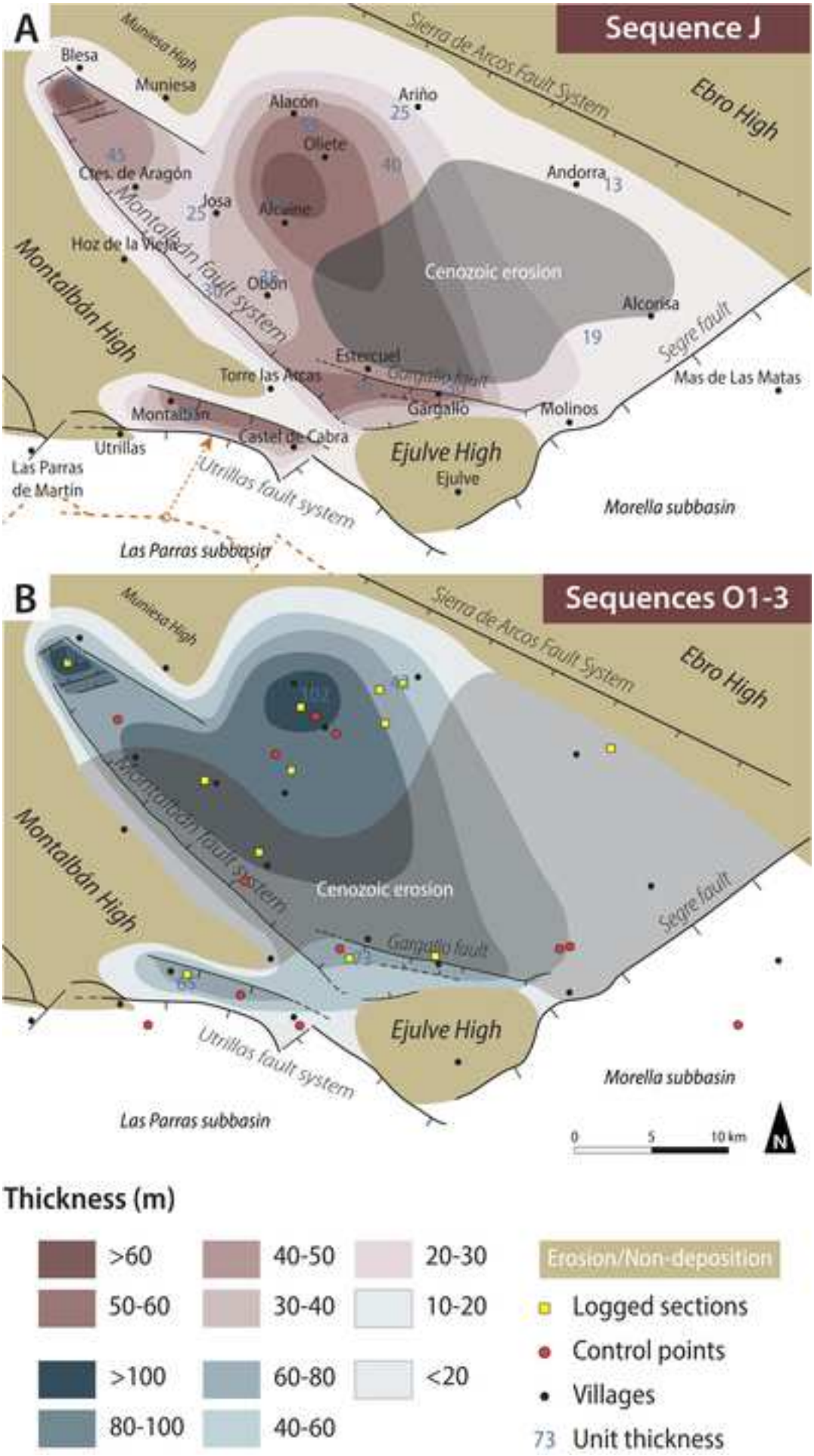

Figure 6

Click here to access/download;Figure;FIg.6.tif

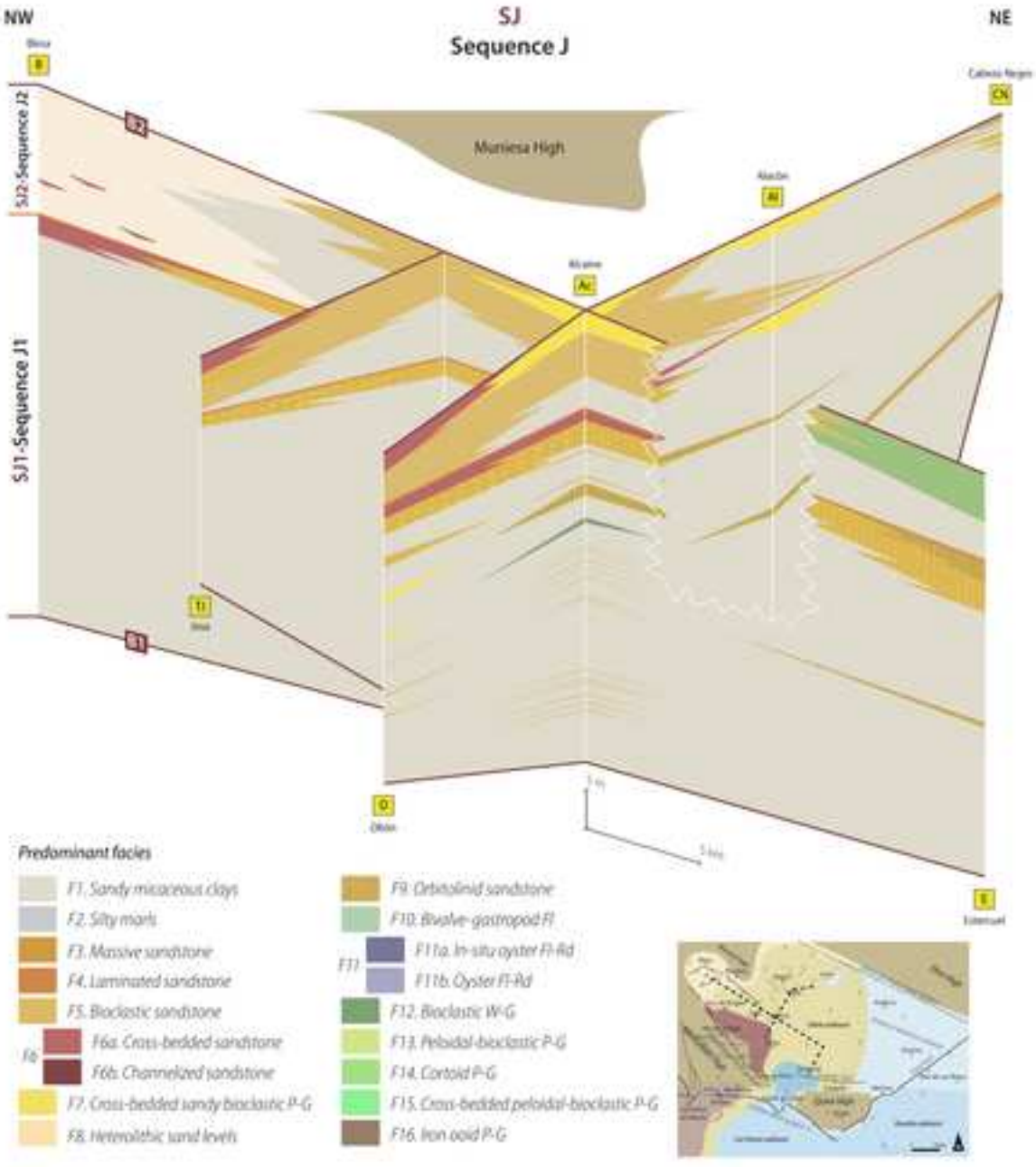

Figure 7

Click here to access/download;Figure;Fig.7.tif

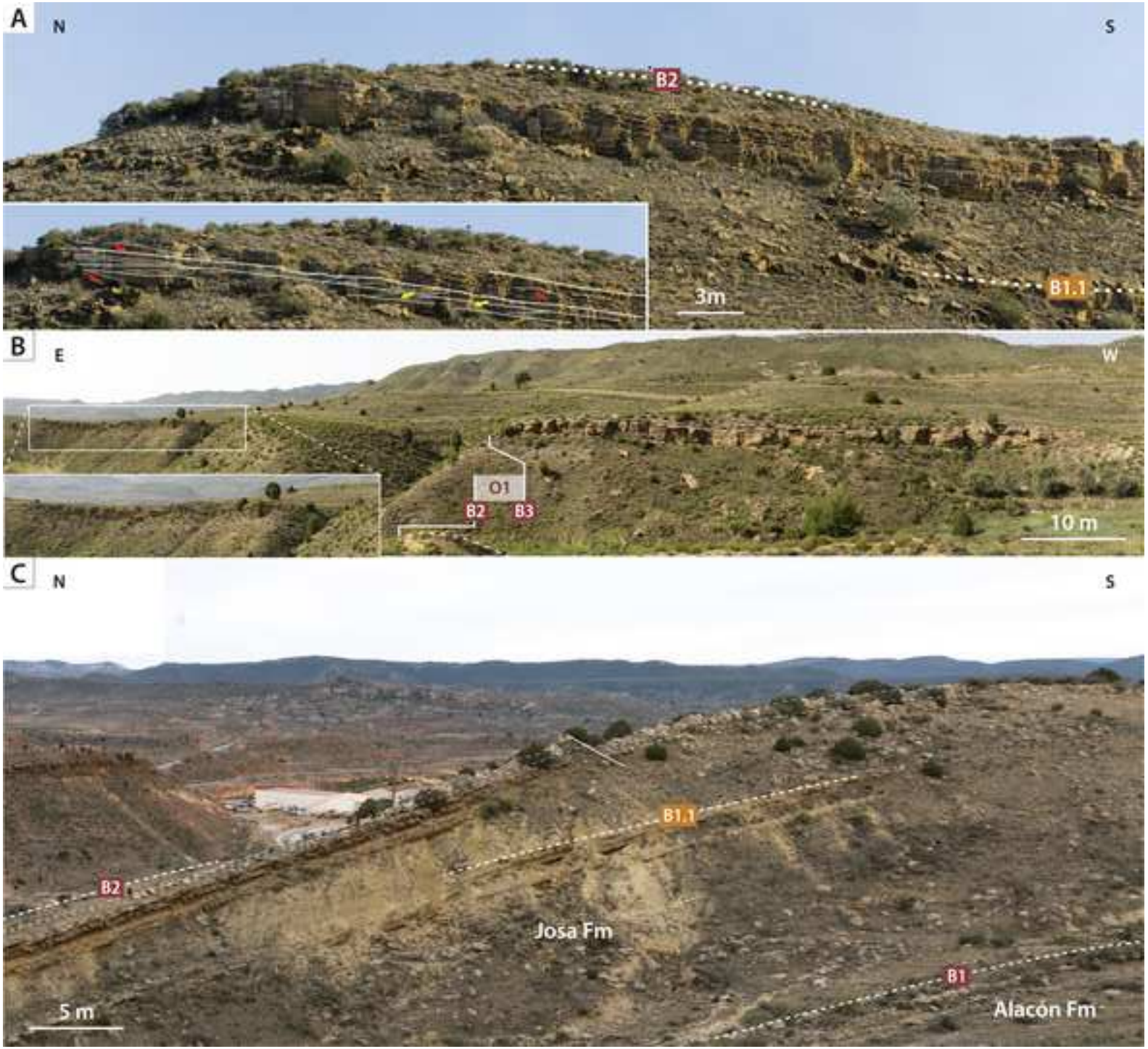

Figure 8

Click here to access/download;Figure;Fig.8.tif

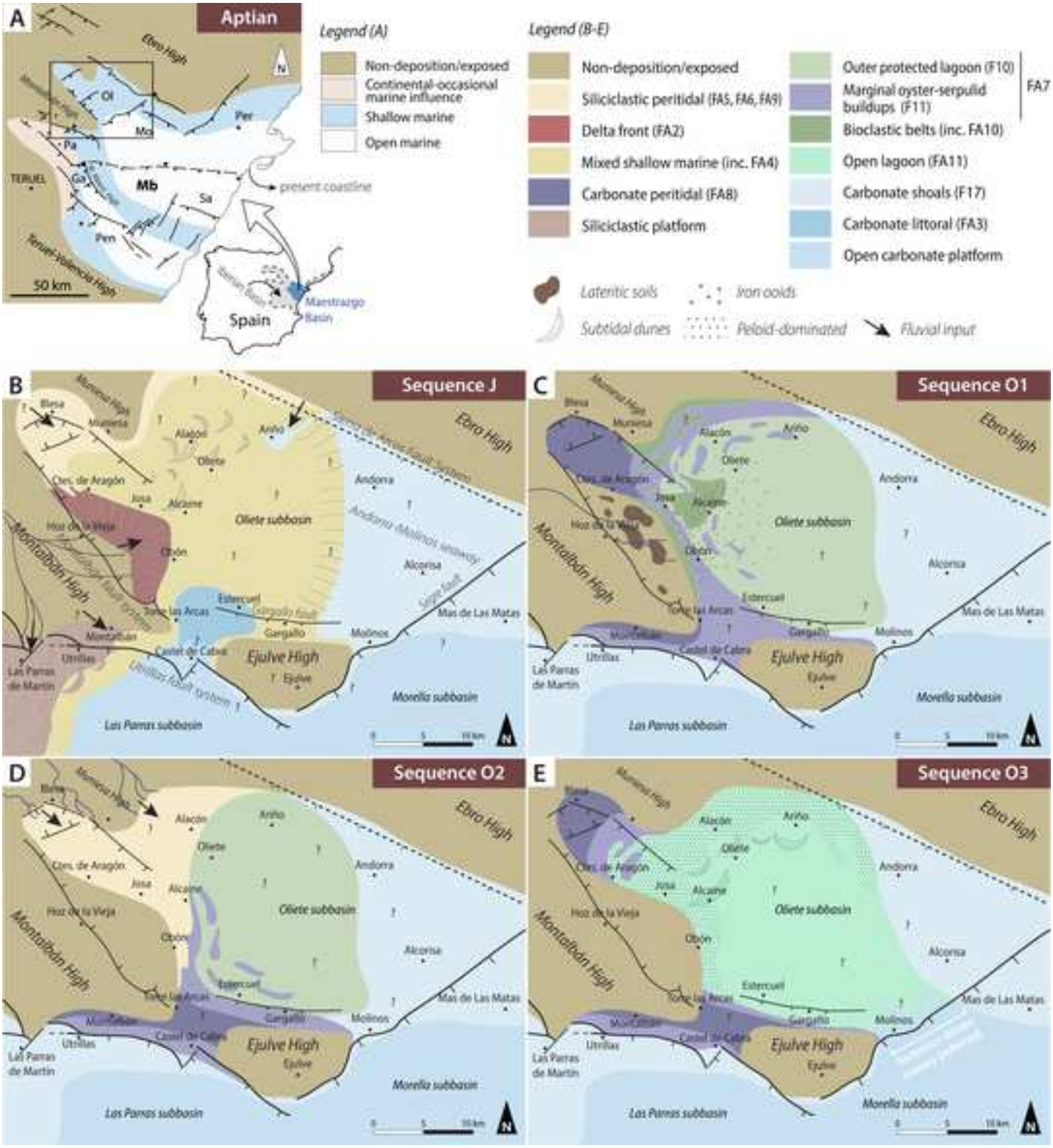

Figure 9

Click here to access/download;Figure;Fig.9.tif

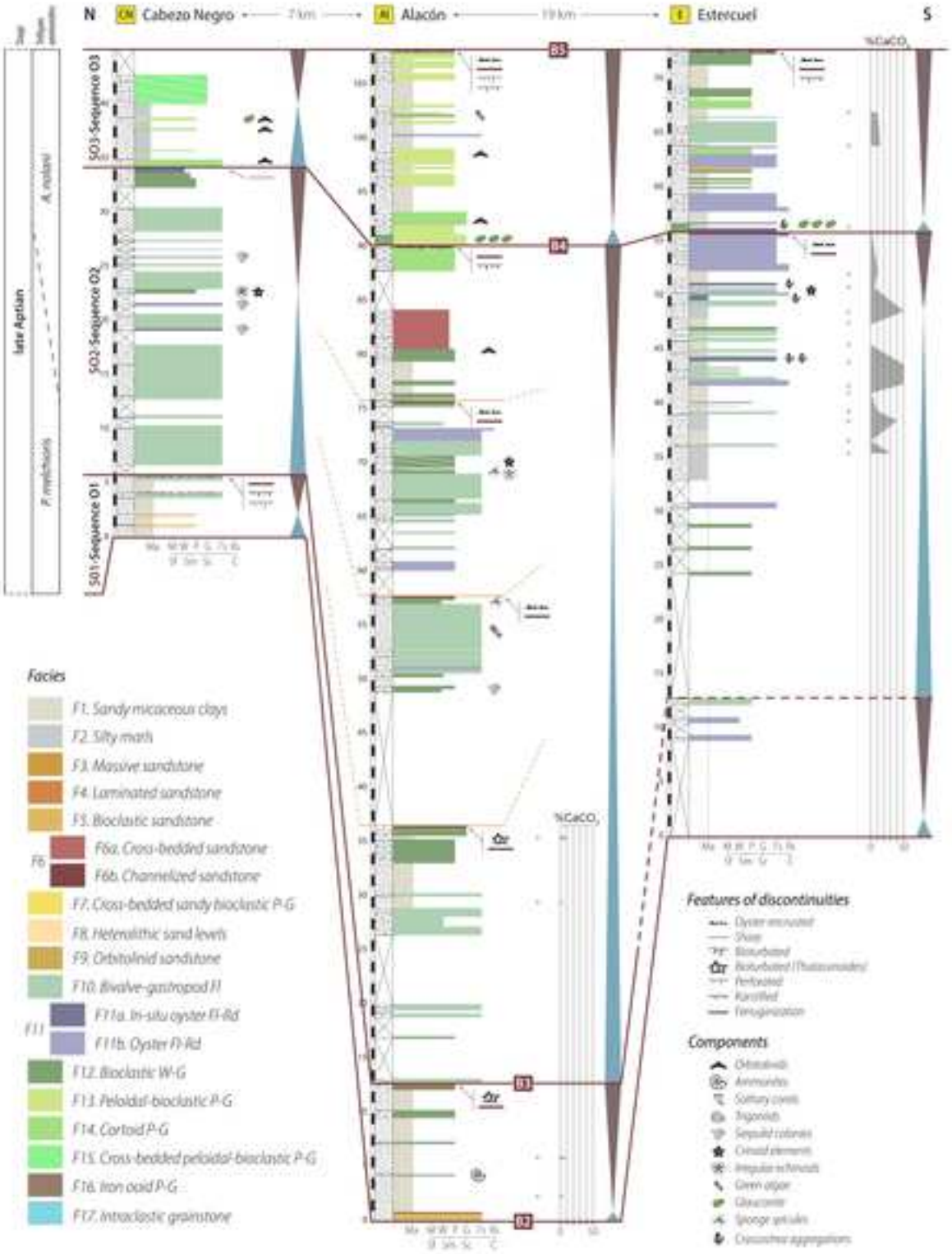

Figure 10

Click here to access/download;Figure;FIg.10.tif

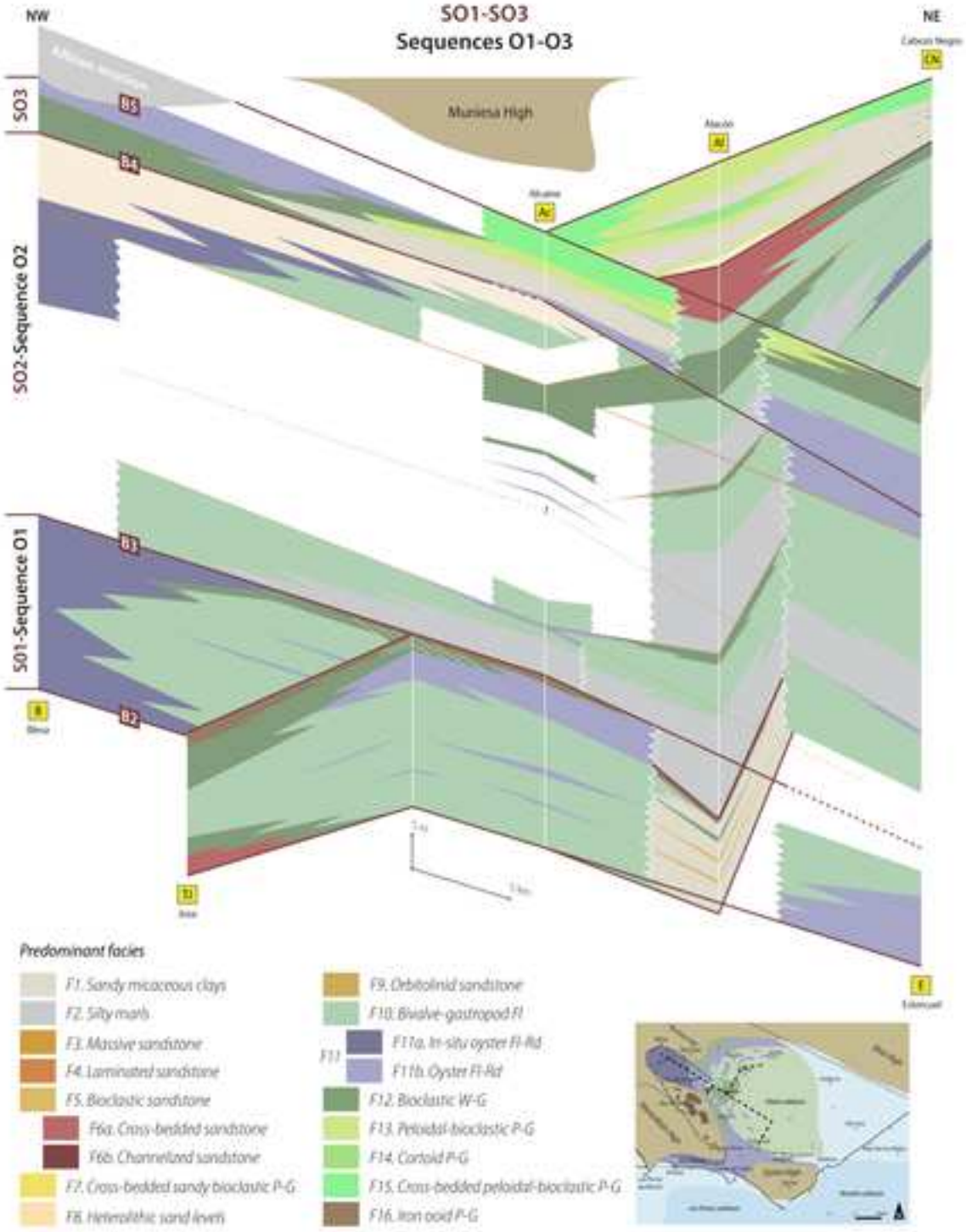

Figure 11

Click here to access/download;Figure;FIg.11.tif

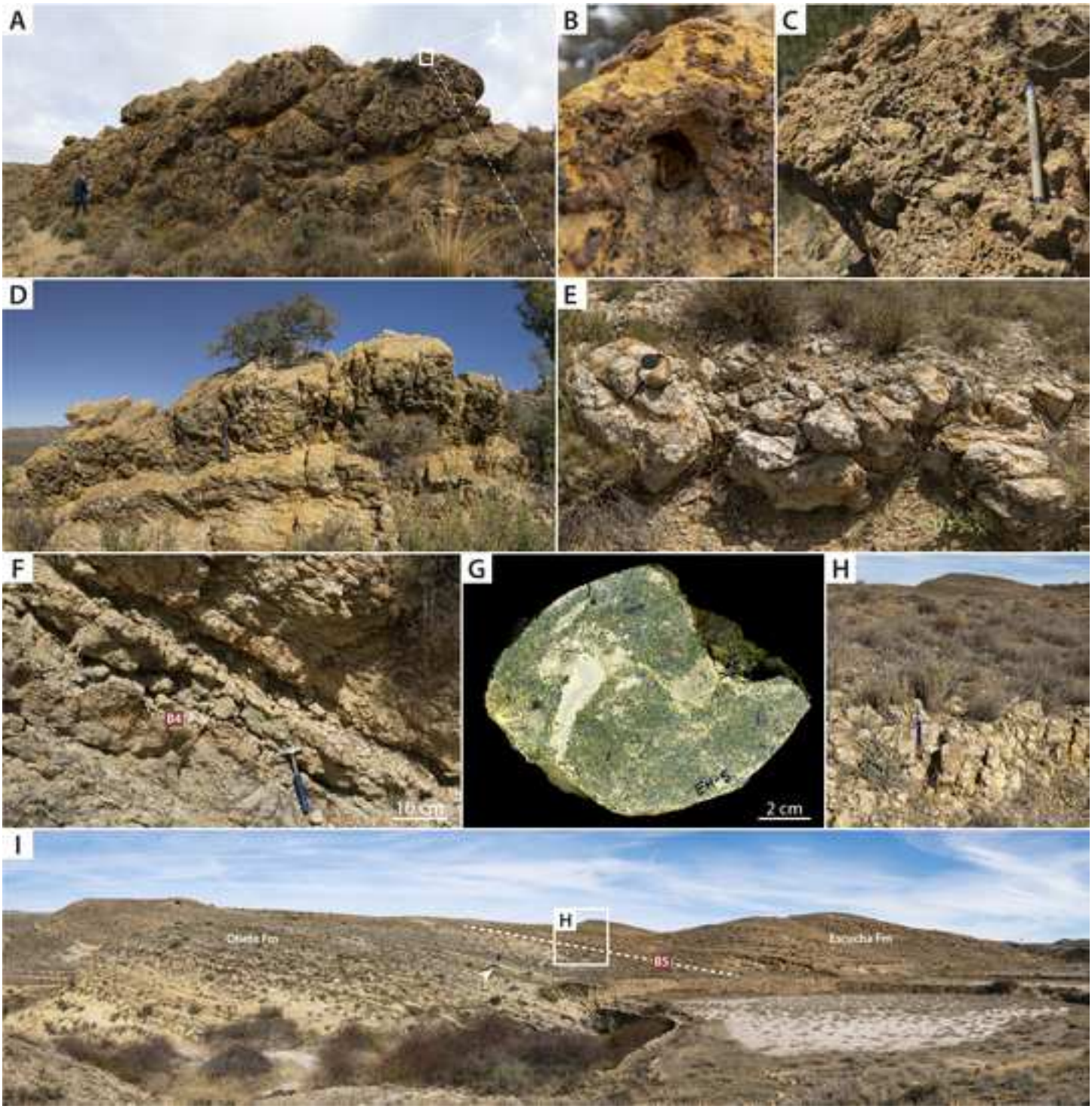

Figure 12

Click here to access/download;Figure;Fig.12.tif

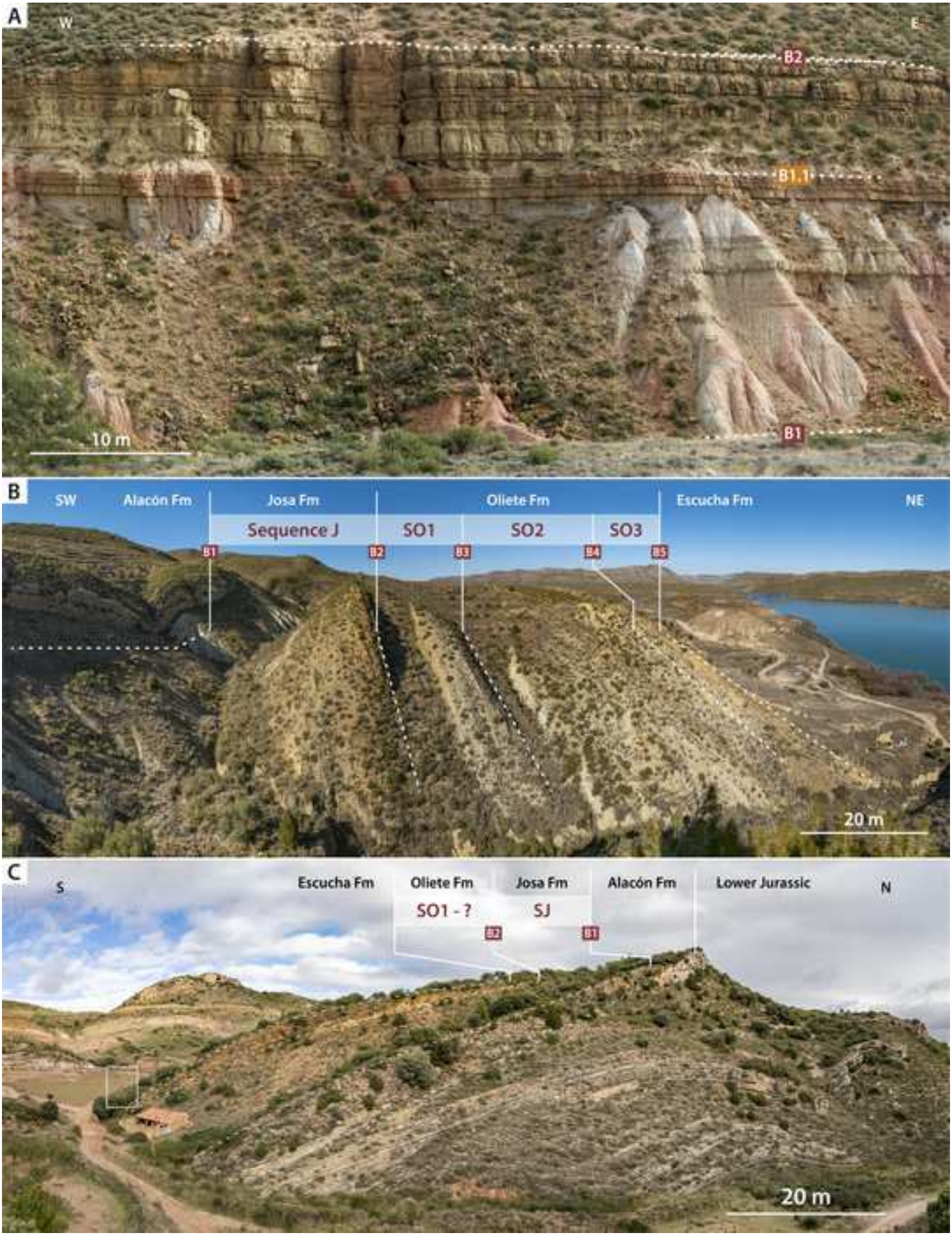

Figure 13

Click here to access/download;Figure;Fig.13.tif

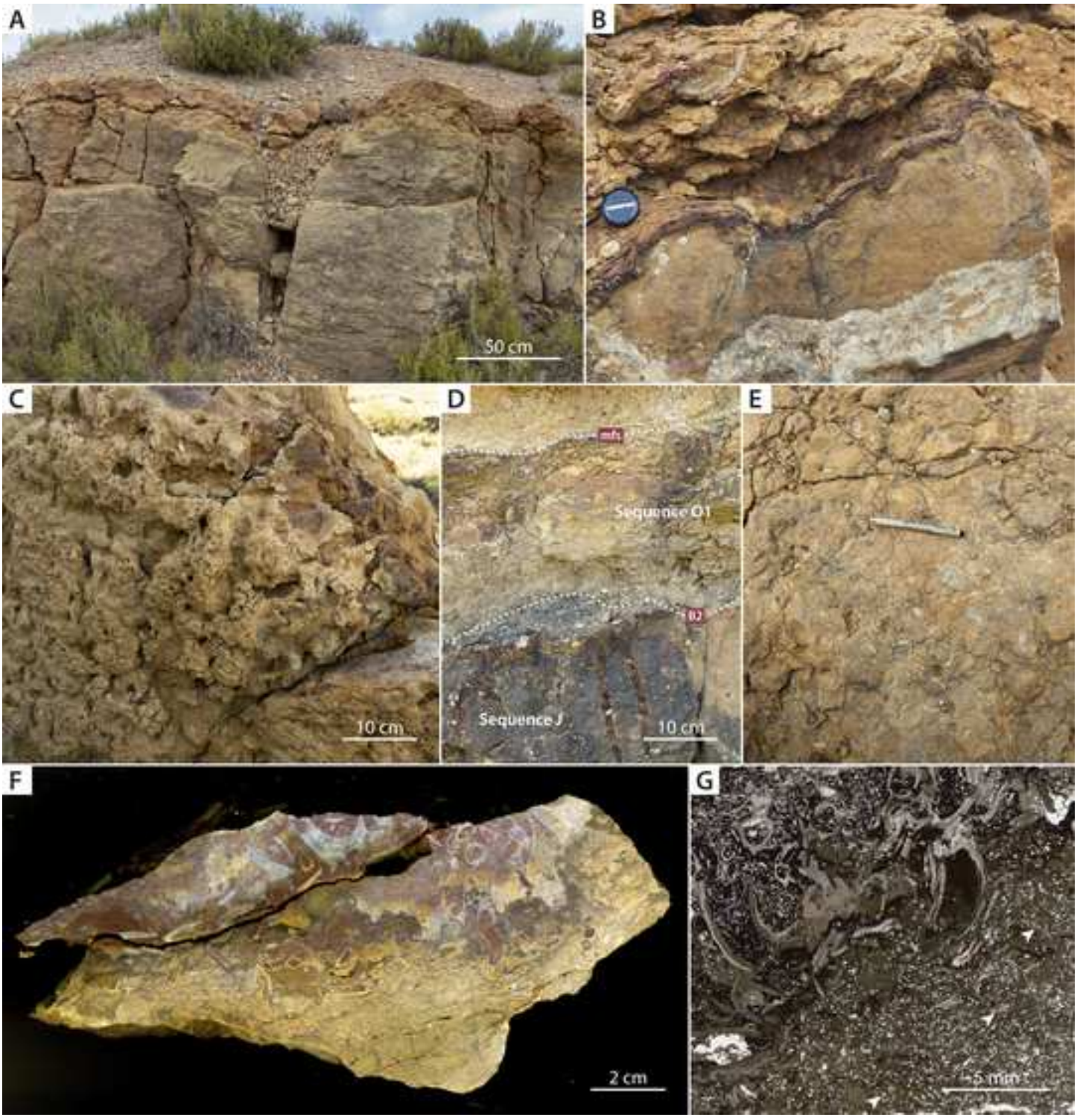

Figure 14

Click here to access/download;Figure;Fig.14.tif

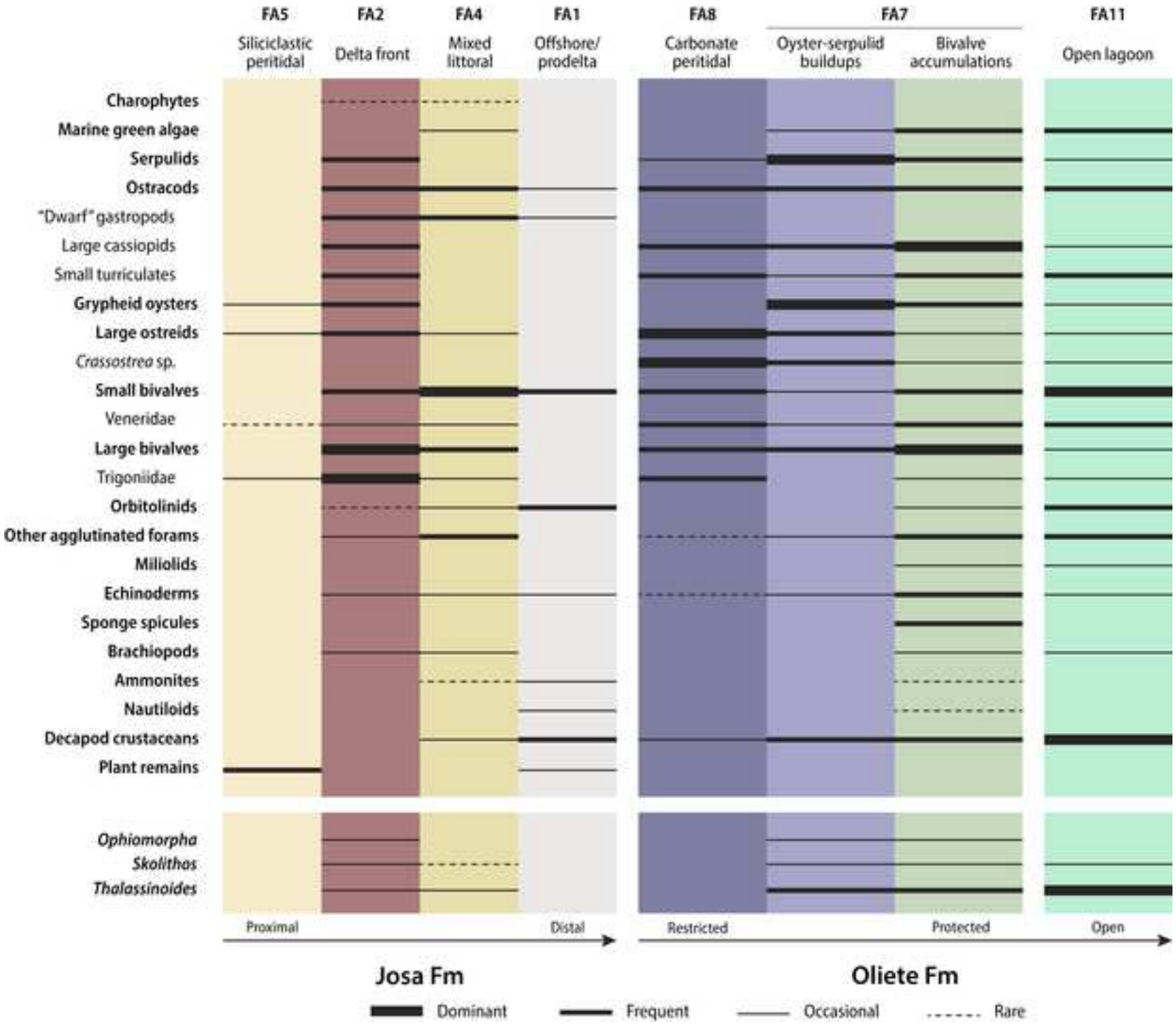

Formation name	**Josa Formation**
Main lithology	**Clays and silts, sandstones and sandy limestones:** White, bluish grey and ochreish marls and lutites with intercalations of fine-grained laminated sandstone, topped by thick medium and coarse-grained sandstones and sandy bioclastic limestones with abundant trigoniids, oysters and other molluscks.
Stratotype	The locality known as Tejería de Josa, northwest of the Josa village (log TJ in Fig. 1C, see also Fig. 12A). *Base*: 40º57'29"N/0º46'55"W; *Top*: 40º57'31"N/0º46'44"W
Facies and thickness	At its type locality, this unit is 39.5 m-thick, with a 31 m-thick basal interval of white to ochreish-reddish, micaceous clays and silts with cm-to-dm-thick intercalations of laminated sands and sandy mudstones. This lower interval is topped by 8.5 m of upwards-coarsening and -thickening levels of sand, sandstone and sandy limestones containing abundant trigoniids. The facies succession of the uppermost Josa Fm is variable across the Oliete Ssubbasin. There is a basinwide transition from levels of massive sandstone and bioclastic sandstone with trough cross-lamination (in the type locality and other marginal localities) towards thick levels of sandy limestone with planar cross-stratification (in depocentral localities). The overall thickness of the unit is variable, reaching a maximum of 66 m at Alacón and a minimum of 25 m at Ariño (Figs. 1 and 3).
Boundaries	*Lower boundary:* discontinuity surface at the top of the underlying Alacón Formation, displaying locally prominent karst features, iron oxide crusts and encrusting organisms. *Upper boundary:* widespread sedimentary discontinuity associated with Fe-oxide staining, recrystallization and localized erosional incision.
Geographical distribution and lateral equivalences (Maestrazgo Basin)	The Josa Fm is present across the Oliete subbasin. Its lateral equivalents in the rest of the Maestrazgo Basin are the upper part of the Forcall Formation and the Villarroya de los Pinares Formation (See Bover-Arnal et al., 2016).
Depositional environment	Mixed carbonate-siliciclastic open ramp, prodelta s.l., delta front.
Age range	Early Aptian, upper *Deshayesites forbesi* to *Dufrenoyia furcata* ammonite biozones.

Table 2

Facies and subfacies		Sedimentary features	Components	
			Skeletal	Non-skeletal
(F1) Pure to calcareous, sandy micaceous clays		m-M to decameterdm-thick tabular levels of white, blue-greay or ochreerish clay with mm-thick silty interbeds	Discoidal orbitolinids, solitary corals, regular and irregular echinoids. Abundant decapod crustaceans, occasionally in carbonate concretions. Scarce ammonoids and nautiloids. Scarce teeth of small shark and durophagous fishes; ostracods, small bivalves (pectinids, gryphaeid oysters). In the Oliete Fm: crinoid stem and arm elements, echinoid plates and spines. Dwarf Tiny pyritized bivalves and gastropods.	Quartz sand, muscovite. Gypsum (In Sequence TJ)
(F2) Silty marls		dDm to m-thick tabular levels beds of greay marls	Ostracods, small bioclasts of oysters, other unidentified bivalves and gastropods.	Variable amounts of quartz silt.
(F3) Massive sandstone		dDm to m-thick tabular to lobe-shaped levels beds of sand and poorly lithified sandstone. Mostly structureless with occasional faint trough cross-lamination.	Mostly azoic unfossiliferous with some bivalve and plant debris.	Fine to medium quartz sand, muscovite.
(F4) Laminated sandstone		cCm to dm-thick tabular levels of fine-grained quartz sandstone with horizontal or hummocky lamination	Rare fragments of oysters and other mollusks	Quartz sand, muscovite.
(F5) Bioclastic sandstone and sandy limestone with large bivalves		cCm to dm-thick tabular levels of quartz sandstone. Locally abundant *Thalassinoides* isp.	Well-sorted, small-sized rounded bioclasts of bivalves, gastropods and serpulids. Rare orbitolinids and echinoid remains. Disarticulated and occasionally articulated thick-shelled bivalves: tT**rigoniids** (*Buchotrigonia, Laevitrigonia, Pterotrigonia, Quadratotrigonia*), aArcids (*Cucullaea*), aArcticids (*Epicyprina*), vVenerids, pPectinids, cCarditids. Frequent **cassiopid** (*Cassiope, Gymnentome*) and **turritellid** gastropods. Only in Sequence O3: very rare radiolitid rudists.	Fine quartz sand, muscovite, occasional phosphatic grains. Occasionally peloids, cortoids.
(F6) Cross-stratified sandstone	**F6a**	dDm to m-thick levels of sandstone with planar or trough cross-stratification. *Ophiomorpha* and *Skolithos* isp. burrows.	Abundant oyster fragments. Bivalve, gastropod and serpulid debris. Scarce echinoderm fragments. Ostracods, scarce charophyte gyrogonites.	Fine to very coarse quartz sand, quartz pebbles, muscovite.
	F6b	Channelized dm-thick levels of sandstone associated to with covered silty intervals		
(F7) Cross-stratified sandy bioclastic P-G		mM-thick levels of planar cross-bedded bioclastic P-G with quartz sand. with planar cross-bedding.	Well-preserved small turriculate gastropods, small bivalves, ostracods and very rare charophyte gyrogonites. Poorly sorted debris of mollusckss, serpulids, agglutinated benthic foraminifera. Accumulations of articulated large bivalves atin the top surfaces of the cross-bedded levels.	Cortoids, small intraclasts. Variable amounts of quartz sand and muscovite.
(F8) Heterolithic sand		mM-thick levels beds of poorly lithified sandstone, siltstone and claystone. Siltstone and claystone levels are usually covered. Sands form massive azoic unfossiliferous levels beds with heterolithic and trough cross-lamination.	AzoicUnfossiliferous	Quartz sand, glauconite, muscovite.
(F9) Orbitolinid sandstone		Tabular, decimetric levels beds of fine quartz sandstone containing abundant discoidal orbitolinids	Large discoidal morphotypes of ***Palorbitolina lenticularis***. Diverse benthic foraminifera (*Neotrocholina, Ackaya minuta, Melathrokeryon, Lenticulina*, miliolids, unidentified biserials), solitary corals, ostracods, calcispheres, dwarf tiny gastropods. Scarce echinoid spicules and plates, and oyster, callianassid and serpulid debris. Rare green algae (*Boueina*) and bryozoan debris.	Quartz sand and silt, muscovite.
(F10) Bivalve-gastropod Fl		Tabular to irregular levels beds of marl, clay marls and nodular limestone containing large articulated bivalves and gastropods, embedded in a mudstonewith a mudstone-to-wackestone bioclastic matrix. Most specimens are preserved as articulated internal moulds. Locally abundant *Thalassinoides isp.* burrows.	Epifaunal bivalves: oOstreids (*Liostrea, Aetostreon,* ***Crassostrea***). Shallow infaunal bivalves, lLucinids (*Sphaera*), aArcticids (*Epicyprina, Proveniella*), vV**enerids** (*Aphrodina, Tapes*), llimids (*Pseudolimea*), scarce cCarditids.. Deep infaunal bivalves: pPholadomyids (*Pholadomya*), hH**iatellids** (*Panopea*). Gastropods: **cassiopids** (*Cassiope, Gymnentome*), **turritellids**, cerithiids, occasional nerineids. Scarce agglutinated benthic foraminifera: *Choffatella decipiens, Ackaya minuta, Charentia.* Frequent Common encrusting serpulids. Variable amounts of debris of bivalves and gastropods, green algae, ostracods, decapods and echinoderms. Rare bryozoans. Very rare and poorly preserved ammonites and nautiloids.	Fine quartz sand, glauconite.
(F11) Oyster Fl-Rd	**F11a**	Tabular to irregular, dm- to m-thick levels beds of floatstones and rudstones integrated bywith large, well-preserved, mostly articulated specimens of	Epifaunal bivalves: *Liostrea,* ***Crassostrea***, *Aetostreon,* frequent lucinids, hiatellids, trigoniids and small **venerids**. Gastropods: frequent common large **cassiopids** and turritellids.	Fine quartz sand and glauconite.

		large oysters, including *Crassostrea* (this taxon is most abundant in Estercuel) and *Aetostreon*. Large individuals of *Crassostrea* occasionally form small ~~in-situ~~ autobiostromes (sequence O2 in Estercuel).	~~Frequent~~ Common gregarious **serpulid colonies**. Undetermined comminuted debris of mollusks and echinoderms. Rare bryozoans.	
	F11b	~~d~~Dm- to m-thick tabular ~~levels~~ beds ~~integrated composed~~ mostly ~~by~~ of tightly packed disarticulated oysters and oyster fragments.	Epifaunal bivalves: disarticulated and broken fragments of oysters (mainly gryphaeids, also ***Crassostrea***, ***Liostrea)*** and other organisms, including turriculate gastropods, bivalves (lucinids, hiatellids, trigoniids, venerids) and echinoderms. Frequent **ostracods** and gregarious **serpulid colonies**.	Fine quartz sand and glauconite.
(F12) Bioclastic W-G		Tabular dm-thick ~~levels~~ beds of fine bioclastic limestone. Occasional *Thalassinoides* traces.	Rounded, moderately well-sorted bioclasts of bivalves and gastropods, ostracods, echinoderms and serpulids. Scarce brachiopods. Occasional serpulid colonies. Locally abundant trigoniids, large oysters and other bivalves. Scarce benthic foraminifera, mostly lituolids. In Sequence O2: locally abundant monaxon sponge spicules.	Peloids, cortoids, intraclasts, fine quartz sand, occasional glauconite. In Sequence O2: occasional micritic rip-up intraclasts and crustacean microcoprolites (*Palaxius* ~~*sp.*~~).
(F13) Peloid-bioclastic W-G		Tabular dm-thick ~~levels~~ beds of fine peloidal limestone with abundant bioclasts. Occasional faint cross-lamination.	Rounded, moderately well-sorted bioclasts of bivalves and gastropods, ostracods, echinoderms and green algae. Rare, rounded fragments of bryozoans. Occasional debris of thick-shelled bivalves and gastropods. Diverse foraminifera, mostly textulariids: *Ackaya, Mayncina, Charentia, Melathrokerion, Lenticulina, Mesorbitolina texana, Haplophragmoides,* miliolids.	Peloids, cortoids, intraclasts, occasional glauconite. Variable amounts of quartz sand.
(F14) Cortoid P-G		Tabular dm-thick levels of cortoidal limestone with abundant bioclasts. Locally abundant *Thalassinoides isp.*	Comminuted and rounded bioclasts of small bivalves, turritellid and cerithiid gastropods, serpulids, echinoderms (*Echinoidea, Crinoidea*) forming the nuclei of cortoids with destructive micritic coatings. Frequent uncoated crinoid elements and green algae debris (mainly *Permocalculus* and *Boueina*). Locally abundant benthic foraminifera: mostly *Choffatella decipiens.* Abundant decapod remains, including *Atherfieldastacus magnus.* In~~n~~ Sequence O3: locally abundant orbitolinids, including *Mesorbitolina texana*.	Cortoids with destructive coatings, intraclasts, quartz sand, peloids. Occasional resedimented ooids and glauconite.
(F15) Cross-bedded peloidal-bioclastic P-G		Tabular dm- to m-thick ~~levels~~ beds of bioclastic-peloidal packstone~~s~~ and grainstone~~s~~ with m-scale planar cross-stratification. Occasional *Thalassinoides* and *Skolithos* isp. ~~traces.~~	Fragmented and rounded bioclasts of small bivalves, oysters, serpulids and red algae. Scarce bryozoan fragments. ~~Frequent~~ Common small turriculate gastropods. Rare brachiopods.	Peloids, cortoids, glauconite, variable amounts of quartz sand.
(F16) Iron ooid W-G		Tabular dm- to m-thick ~~levels~~ beds of bioclastic packstones and grainstones with abundant ferruginous ooids. o. Occasionally form~~s~~ing lobe-shaped bodies with low angle cross-stratification.	~~Frequent~~ Common cementing **oysters**, bioclasts of small **bivalves**, **gastropods**, echinoderms, red algae. Occasional otracods and lituolids. Rare callianassid remains.	Ferruginous ooids, cortoids.
(F17) Intraclastic P-G		m-~~M~~ to ~~decameter~~dm-thick, occasionally lobe-shaped ~~levels~~ beds of intraclastic grainstones with planar cross-bedding.	Fragments of oysters and other bivalves.	Intraclasts, cortoids.

Formatted: Font: Not Italic

Declaration of interests

☒The authors declare that they have no known competing financial interests or personal relationships that could have appeared to influence the work reported in this paper.

☐The authors declare the following financial interests/personal relationships which may be considered as potential competing interests: